To the Graduate Council:

I am submitting herewith a thesis written by Dustin Holt Crider entitled "Determination and Analysis of the Spectral Emissivity of a Blackbody Simulator Source." I have examined the final electronic copy of this thesis for form and content and recommend that it be accepted in partial fulfillment of the requirements for the degree of Master of Science, with a major in Engineering Science.

L. Montgomery Smith
_____

Major Professor

We have read this thesis
and recommend its acceptance:

Roy Schulz
_____

Basil Antar
_____

Accepted for the Council:

Anne Mayhew
_____
Vice Chancellor and
Dean of Graduate Studies

(Original signatures are on file with official student records.)

DETERMINATION AND ANALYSIS OF THE SPECTRAL EMISSIVITY OF A BLACKBODY SIMULATOR SOURCE

A Thesis
Presented for the
Master in Science
Degree
The University of Tennessee, Knoxville

Dustin Holt Crider
August 2006

ACKNOWLEDGEMENTS

I wish to thank all those aided me in the completion of this thesis. In particular, I thank my advisor, Dr. Smith. His thoroughness and attention to detail were a vital part of this thesis. I also thank my committee members, Dr. Antar and Dr. Schulz, for their assistance. Appreciation is also due to several of my coworkers and colleagues for helping me to complete the work: Carl Brasier, Ken Bynum, Stuart Coulter, David Crandall, Heard Lowry, Joel Mansfield, Kim Mead, Randy Nicholson, Annette Painter, Sid Steely, and Ray Young. Above all, I praise and thank the Triune God of the Bible, because only in His light, do we see light (Psalm 36:9).

Approved for public release; distribution is unlimited

ABSTRACT

Blackbody simulator sources used for calibration of electro-optical sensors must be well characterized, especially in regards to source emissivity. Many applications require only the total emissivity to be known, but the motivation behind this present research required the spectral emissivity to be determined. Thus, theoretical and experimental methods for ascertaining the spectral emissivity of a blackbody simulator were investigated. Based on the blackbody simulator cavity geometry and material, the methods of Gouffé, Kelly, and Bartell [1] were used to calculate the theoretical spectral emissivity. The experimental phase of this study involved using two Fourier Transform Infrared (FTIR) instruments to measure the simulator spectral emissivity. A spectral emissometer, called the Optical Properties Measurement System (OPMS) was first used. Then, a spectral reflectometer, called the Scatterometer/Reflectometer (SCAT/R), was used to measure the spectral reflectance of the blackbody simulator cavity. The emissivity was then calculated from the reflectance data using Kirchoff's Law. An extensive error analysis performed on the experimental emissivity data sets showed the OPMS data to have better quality than the SCAT/R data, with maximum standard deviations of 4.70×10^{-3} and 2.69×10^{-2}, respectively. The theoretical and measured emissivities were compared and showed that Kelly's theory compared the best with the OPMS measurements, with differences on the order of 0.1%. Finally, the measurement uncertainties were translated into an uncertainty in the measured output of the blackbody simulator, which was 2% and 3.2% for the OPMS and SCAT/R respectively.

TABLE OF CONTENTS

CHAPTER **PAGE**

1.0 INTRODUCTION 1

1.1 Introduction to the 7V Chamber 1

1.2 Purpose of Thesis 3

1.3 Standard Infrared Sources 4

1.4 Summary of Work Performed 6

2.0 BACKGROUND 9

2.1 Blackbody Radiation Theory 9

2.2 Blackbody Simulator Cavity Theory 12

2.3 FTIR Spectrometry Background 19

2.4 AEDC FTIR Instruments 22

2.4.1 Optical Properties Measurement System 22

2.4.2 Scatterometer/Reflectometer 26

2.5 Summary 29

3.0 METHODS FOR DETERMINING SPECTRAL EMISSIVITY 30

3.1 Theoretical Methods 30

3.2 OPMS Measurement Method 34

3.3 SCAT/R Measurement Method 36

3.4 Uncertainty Analysis Method 39

3.5 Relation of Measurements to 7V Standard Source 41

4.0 THEORETICAL AND EXPERIMENTAL RESULTS 43
4.1 Theoretical Results.....43
4.2 OPMS Measurements 43
4.2.1 Results.....43
4.2.2 OPMS Data Uncertainty Analysis 47
4.2.3 Comparison of Measurements and Theories.....51
4.3 SCAT/R Measurements 53
4.3.1 Results.....53
4.3.2 SCAT/R Data Uncertainty Analysis 56
4.3.3 Comparison of Measurements and Theories.....59
4.4 Relation of Measurement Uncertainty to Effective Radiance 60

5.0 SUMMARY AND CONCLUSIONS 64

REFERENCES 66

VITA 71

LIST OF TABLES

TABLE **PAGE**

1. Theory Summary 19

2. SCAT/R Detectors 27

3. Comparison of Total Emissivities.....34

4. Summary of Effective Radiances.....62

5. Measured Standard Source Effective Radiance Data Taken in 7V Chamber.....63

LIST OF FIGURES

FIGURE **PAGE**

1. High-Level 7V Chamber Block Diagram 2
2. Calibration Monitor System 2
3. Calibration Scheme 3
4. SIRSIII Cavity with Reentrant Cap On and Off 5
5. SIRSIII Cavity Design 6
6. Spectral Radiant Exitance 10
7. Cavity of Arbitrary Shape 13
8. Simple Cavity Configurations 14
9. Reentrant Cone Configuration 14
10. Projected Solid Angle 15
11. Reentrant Cavity Geometric Definitions 18
12. Michelson Interferometer 21
13. Optical Properties Measurement System 23
14. OPMS Schematic 23
15. OPMS Measurement Process 25
16. SCAT/R Instrument 26
17. SCAT/R Schematic 28
18. Anodized Aluminum Hemispherical Spectral Emissivity 30
19. SIRSIII Total Emissivity Calculation Process 33
20. Averaged Spectral Reflectivity for Open Port on SCAT/R 38
21. Theoretical Spectral Emissivity with Reentrant Cap 44

22. Theoretical Spectral Emissivity without Reentrant Cap 44

23. OPMS Measured Spectral Emissivity with Reentrant Cap On.....45

24. OPMS Average Measured Spectral Emissivity with Reentrant Cap On 45

25. OPMS Measured Spectral Emissivity with Reentrant Cap Off 46

26. OPMS Average Measured Spectral Emissivity with Reentrant Cap Off 47

27. OPMS Type A Uncertainty – Cap On 48

28. OPMS Type A Uncertainty – Cap Off.....49

29. OPMS Combined Standard Uncertainty – Cap On.....50

30. OPMS Combined Standard Uncertainty – Cap Off.....51

31. Comparison of OPMS Measurements to Theory – Cap On 52

32. Comparison of OPMS Measurements to Theory – Cap Off.....52

33. SCAT/R Measured Spectral Emissivity with Reentrant Cap On.....54

34. SCAT/R Average Measured Spectral Emissivity with Reentrant Cap On 54

35. SCAT/R Measured Spectral Emissivity with Reentrant Cap Off 55

36. SCAT/R Average Measured Spectral Emissivity with Reentrant Cap Off 55

37. SCAT/R Type A Uncertainty – Cap On 56

38. SCAT/R Type A Uncertainty – Cap Off.....57

39. SCAT/R Combined Standard Uncertainty – Cap On 58

40. SCAT/R Combined Standard Uncertainty – Cap Off.....58

41. Comparison of SCAT/R Measurements to Theory – Cap On 59

42. Comparison of SCAT/R Measurements to Theory – Cap Off.....60

43. OPMS Data Uncertainty Effect on Effective Radiance.....61

44. SCAT/R Data Uncertainty Effect on Effective Radiance.....61

CHAPTER I

INTRODUCTION

1.1 Introduction to the 7V Chamber

For over three decades, the space simulation chambers in the Space Systems Test Facility (SSTF) at the Arnold Engineering Development Center (AEDC) have been used to perform characterization, calibration, and mission simulation testing of space-based, interceptor, and airborne electro-optical sensors. These chambers provide a significant ground test capability for radiometric characterization, goniometric evaluation, and mission scenario simulation for sensor systems [2], [3]. The 7V Chamber in particular has been the primary sensor calibration facility at AEDC since the early 1970's and has supported the testing of over 48 sensors. The chamber can provide a variety of tests to perform calibrations and evaluate sensor performance [4].

A high-level block diagram of the 7V Chamber is shown in Figure 1. The chamber has a variety of source systems to project various scenes and targets to the sensor under test (SUT). A flat mirror folds the radiation from the sources to a two mirror collimating system after which the radiation is directed toward the SUT. A translatable mirror is also available to redirect the radiation into the Calibration Monitor System (CMS), shown in Figure 2. The CMS houses a single-element Arsenic-doped Silicon (Si:As) detector that is calibrated using the 7V Standard Source blackbody simulator which was calibrated at the National Institute of Standards and Technology (NIST). The Si:As detector is then used to calibrate the other blackbody simulator sources in the chamber. The calibration scheme is shown in Figure 3.

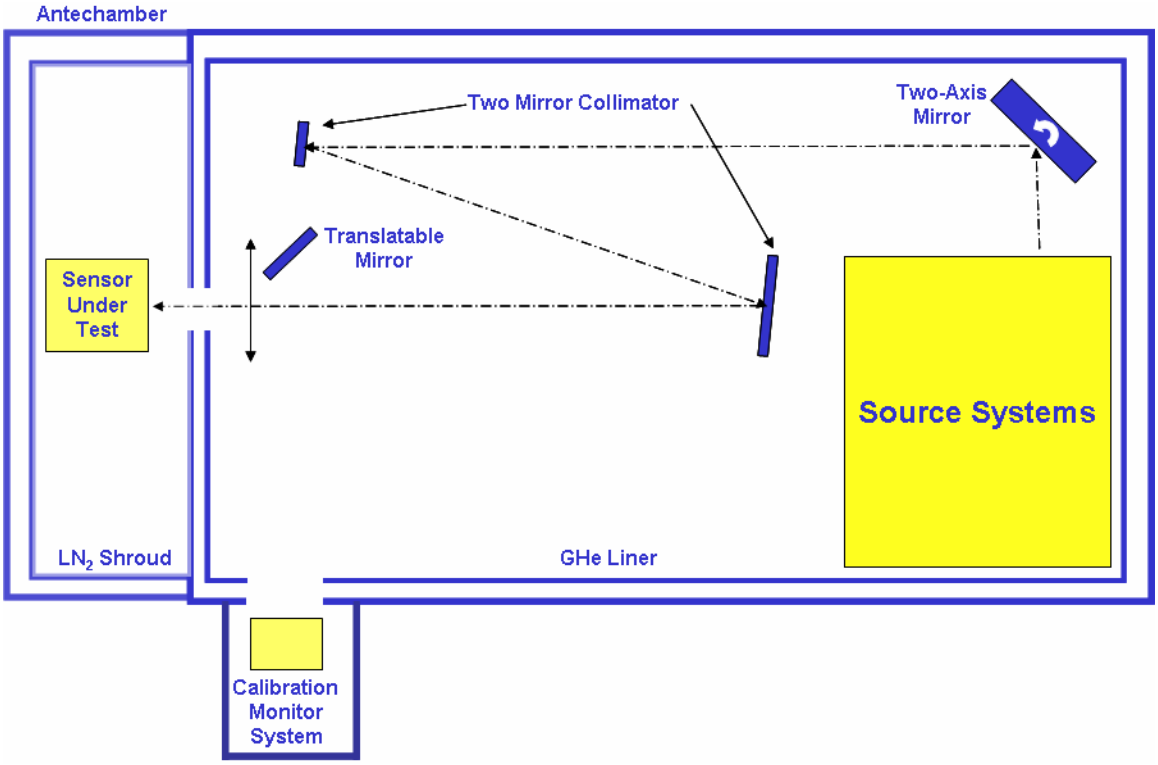


Figure 1. High-Level 7V Chamber Block Diagram

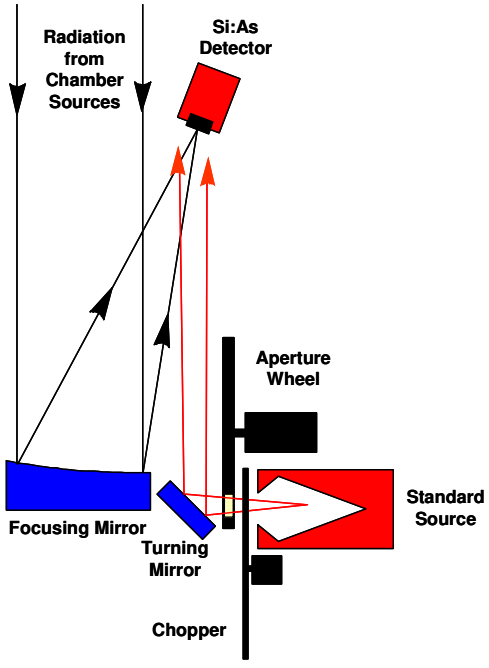


Figure 2. Calibration Monitor System

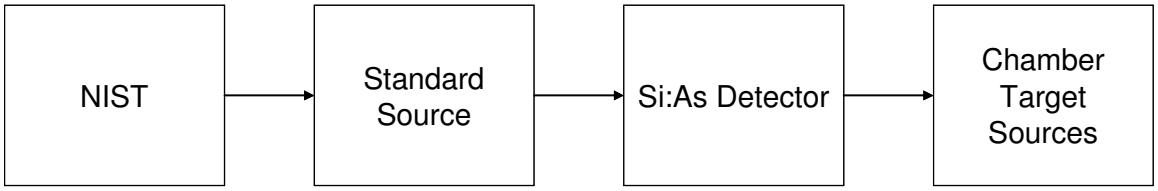


Figure 3. Calibration Scheme

The main chamber is 7 ft in diameter and 21 ft long and contains a light-tight, cryogenically cooled liner (20 K), which is essential for simulation of the low radiometric background of space. The pumping system can attain a pressure of less than 10^{-7} torr, which is equivalent to a 200 mile altitude on standard atmosphere. The chamber is housed within a recently refurbished class 1,000 clean room. It is vibration isolated via an airbag suspension system and in concert with the rigid design of the optical bench, provides an optical line-of-sight vibrational stability of 3.5 μrad.

1.2 Purpose of Thesis

To keep pace with evolving sensor missions and technologies, capability upgrades to the 7V Chamber are continuously pursued and implemented [5], [6]. These upgrades require rigorous facility characterization and calibration activities that are part of AEDC's annual activities to comply with Major Range Test Facility Base (MRTFB) processes to ensure quality metrology and test data.

Thus, there is an ongoing effort to build a high-quality verification and validation (V&V) program for the 7V simulation and measurement systems. This effort includes detailed uncertainty analyses and radiometric modeling of the all sources and the optical systems [7]. Blackbody simulator sources are an integral part of the 7V systems and

serve a variety of target and calibration functions. The analysis and modeling of these sources are very important, especially since they are a major contributor to calibration uncertainty [8]. Accurate modeling identifies the system components and illustrates how each contributes to the radiometric throughput and uncertainties that can affect test results. The radiometric properties of these components need to be well understood and documented in order to provide precise calibration data.

Two radiometric properties of the sources used in the 7V Chamber that need to be understood are the total and spectral emissivity. The emissivity dictates how closely a source approximates a true blackbody, and should be quantified because in order to evaluate a sensor's response to stimuli, the stimuli must be well known. The methods used to model and validate the source performance must also be accurate. In particular, the Standard Source in the 7V Chamber is a component that needs to be well characterized, as it serves as the basis of calibration for the detector and all the other blackbody sources. The purpose of the present thesis was to investigate the ability of the Standard Source to emit blackbody radiation across the spectrum for calibration and measurement V&V. The 7V Chamber Standard Source will be described in more detail in the next section.

1.3 Standard Infrared Sources

In the early 1980's, AEDC began to develop cryogenic, vacuum rated, low temperature blackbody simulator sources for calibration purposes that became known as the Standard Infrared Sources (SIRS) [9]. The first two generations of these sources had a temperature range of 100 to 400 K, which was mainly limited by the outgassing of the

materials used in the construction. The current technology level Standard Source, called the SIRSIII, has a temperature range of 150 to 500 K. The SIRSIII has a conical aluminum cavity with a black anodized interior surface. An aluminum reentrant cap is used to increase the effective emissivities of the source, both spectrally and totally. The effective increase in emissivity due to reentrant designs as opposed to simple conical cavity designs has been demonstrated theoretically and experimentally [10], [11]. Figure 4 shows the cavity with the reentrant cap on and screwed off.

The cavity geometry is shown in Figure 5. The vertex angle of the cone is 18 degrees and the reentrant cap has an angle of 45 degrees [9]. When the source was designed, its effective total emissivity was calculated according to the Gouffé Method (to be described in the next chapter) to be greater than 0.999 [9] but it has never been verified or validated. The output aperture diameter is 0.53 cm (0.21 in.). The cavity is heated with constantan wire wound along grooves in the core in a manner that provides uniform cavity heating. Constantan is an alloy of 45% nickel and 55% copper and is known for its nearly constant resistance when subject to temperature variations.

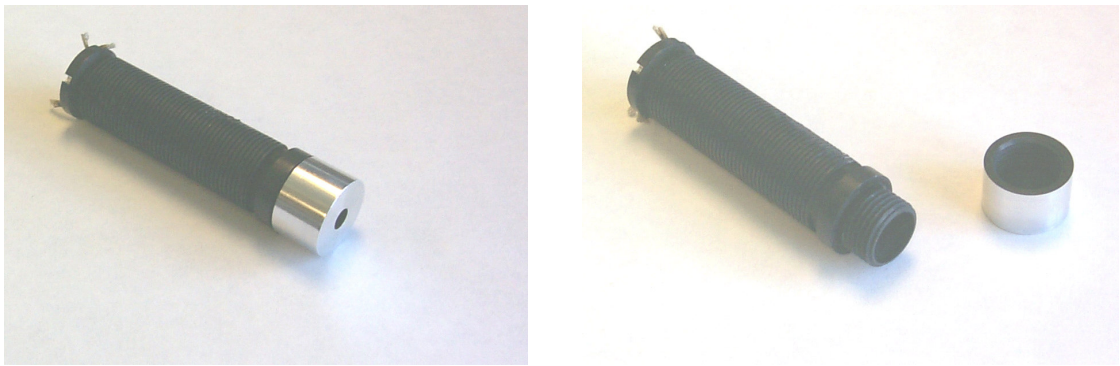


Figure 4. SIRSIII Cavity with Reentrant Cap On and Off

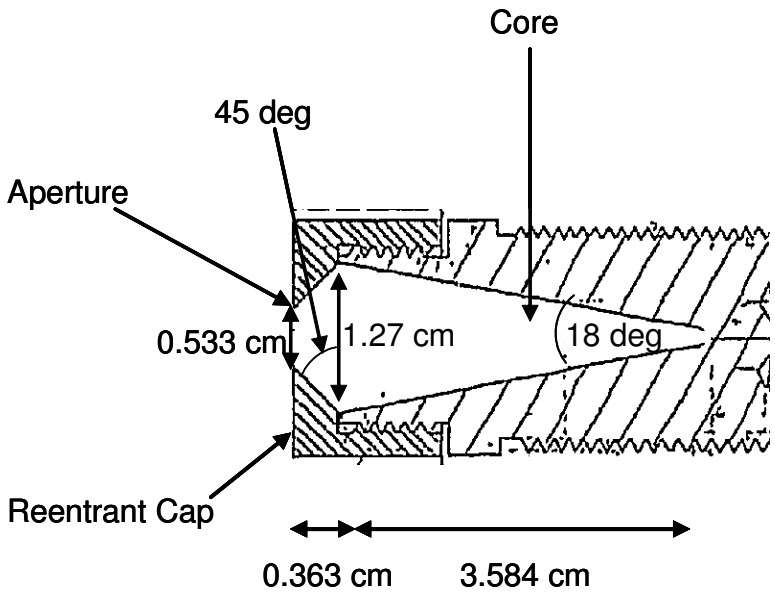


Figure 5. SIRSIII Cavity Design

1.4 Summary of Work Performed

The work in this thesis was initiated to answer the need to characterize and determine both the spectral emissivity distribution over the wavelength range 2 to 20 μm, as well as the total effective emissivity of the Standard Source. The first phase of this work consisted of an extensive literature search to find relevant published work in this area. Very little work on spectral emissivity characterization and measurement of blackbody simulator cavities was found.

There is much literature, however, on the theory and measurement of the total emissivity from blackbody simulators [1]. There is also much work published on spectral emissivity measurements of materials, especially measurements that use Fourier Transform Infrared (FTIR) spectrometry [12], [13], [14]. Since blackbody simulator cavities are designed to be very low reflecting (quality devices having reflectivity on the

order of 0.001), this makes a spectral reflection measurement to derive the spectral emissivity very challenging for blackbody simulators. For most radiometric applications, only the total emissivity of blackbody simulators is needed. These reasons explain why there is very little work published on cavity spectral emissivities. NIST has reported that they have constructed a facility for performing infrared spectral emissivity measurements and have done so on a blackbody simulator [15]. The paper does not give any details on the blackbody simulator design nor does it show any comparison with theoretical spectral emissivity calculations. The NIST measurements were performed at a temperature of approximately 930 K. Some theoretical consideration of the spectral emissivity of blackbody simulators has also been performed using Monte Carlo methods [16]. These analyses were performed at temperatures greater than 1000 K and were not compared to well known emissivity theories or experimental data. Thus, there is a lack of practical comparisons between spectral emissivity theoretical and experimental data in the published literature.

The next part of this study involved investigating the foundational theory of blackbody radiation. This was extended to a theoretical analysis of blackbody hardware and design. A SIRSIII cavity was obtained and efforts begun to better characterize the emissive properties of blackbody simulator design. First, based on the cavity geometry and anodized aluminum spectral emissivity data, three methods were used to calculate theoretical spectral emissivities. These methods are named after their originators, Gouffé, Kelly, and Bartell [1]. The anodized aluminum data was input into the theoretical equations and an effective cavity spectral emissivity was calculated. These theories are normally used for calculating total emissivity but were extended in this study

to predict spectral emissivity. For the experimental phase, two experiments using two different instruments at AEDC were set up and measurements were performed. An instrument called the Optical Properties Measurement System (OPMS) was first used to measure the SIRSIII cavity effective spectral emissivity. The OPMS measures spectral reflectivity and calculates spectral emissivities based on Kirchoff's Law [1]. A spectral reflectometer, called the Scatterometer/Reflectometer (SCAT/R), was the second instrument used to measure the spectral reflectance of the SIRSIII cavity. Then, the measured reflectance data was used to calculate the cavity effective spectral emissivities based on Kirchoff's Law. The theoretical and measured spectral emissivities were compared. An extensive error analysis was performed on the measured emissivity data sets. The uncertainty in the emissivity measurements were then used to estimate the uncertainty in the measured output of the Standard Source. The results of the theoretical analyses are consistent with the published literature and demonstrated the excellent design of the blackbody source cavity. The scans made with the OPMS correlate to the theoretical data very well, with differences on the order of 0.5%. The reflectometer measurements were not however, as good, mainly due to the fact that the instrument was not intended to be used for emissivity measurements. However, both emissivity measurement methods demonstrated the high emissivity of the cavity.

CHAPTER II

BACKGROUND

2.1 Blackbody Radiation Theory

German physicist Max Planck developed the theoretical expression for blackbody radiation [17]. His equation gives the energy per unit volume per unit wavelength, or the spectral energy density, denoted by P(λ), in units of J/m^3/m. The Planck Radiation Law is given by

$$P(\lambda) = \frac{8 \cdot \pi \cdot h \cdot c}{\lambda^5 \cdot \left(e^{\frac{h \cdot c}{\lambda \cdot k \cdot T}} - 1 \right)}, \tag{1}$$

where h is Planck's constant, which is 6.626 x 10^{-34} W s^2, c is the speed of light, 2.998 x 10^8 m/s, λ is the wavelength of the radiation, k is Boltzmann's constant, which has a value 1.381 x 10^{-23} J/K, and T is the absolute temperature [18], [19]. The practical applications of this theory will now be discussed.

Radiant exitance is the term for radiation that is emitted from an object in an 180^o hemisphere per the emitting area [20]. This quantity is typically used when dealing with infrared sources, such as those used in the 7V Chamber. From the Planck Law for perfect blackbody emitters, the spectral radiant exitance is given by

$$M_e(\lambda) = \frac{2 \cdot \pi \cdot h \cdot c^2}{\lambda^5 \cdot (e^{\frac{h \cdot c}{\lambda \cdot k \cdot T}} - 1)}, \tag{2}$$

where λ is the emitted wavelength of the radiation, T is the absolute temperature of the

blackbody in Kelvin, h is Planck's constant, c is the speed of light, and k is Boltzmann's constant. The units of $M_e(\lambda)$ are W/m^2/m. This equation can be reduced to the form

$$M_e(\lambda) = \frac{3.74 \cdot 10^4}{\lambda^5 \cdot (e^{\frac{14388}{\lambda \cdot T}} - 1)}, \tag{3}$$

which has units W/cm^2/μm. Figure 6 shows the theoretical spectral radiant exitance for blackbodies with temperatures of 300, 500, and 800 K.

Assuming a Lambertian radiator, where the radiation intensity is dependant on the cosine of the viewing angle, the radiance, L_e, is related to the radiant exitance according to the equation [20]

$$M_e = \pi \cdot L_e . \tag{4}$$

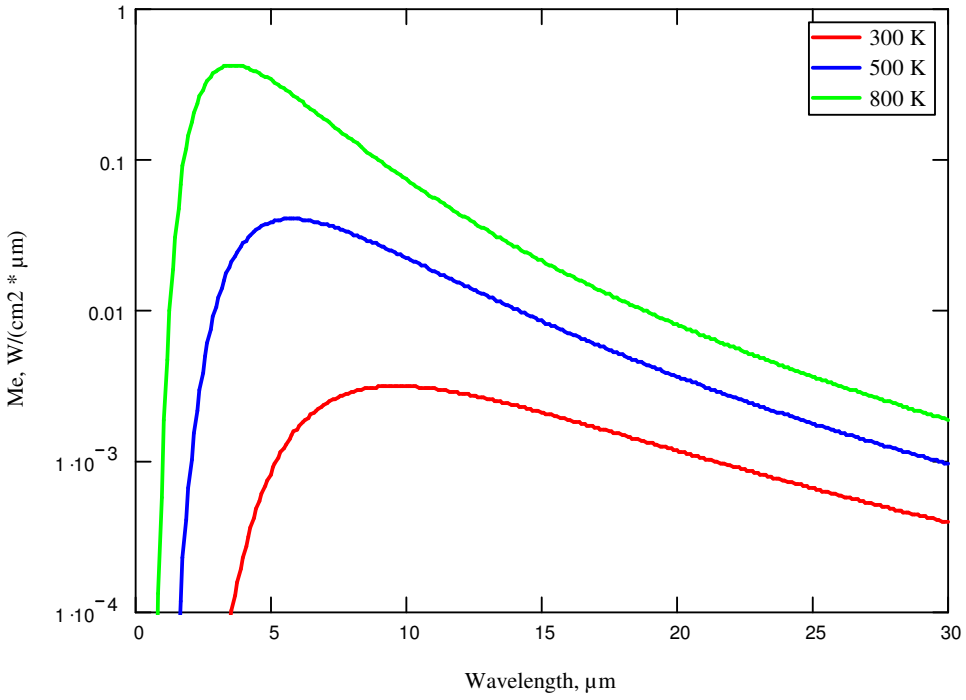


Figure 6. Spectral Radiant Exitance

The Stefan-Boltzmann Law gives the total blackbody exitance over all wavelengths for a given blackbody temperature, T.

$$M_{total} = \sigma \cdot T^4 \tag{5}$$

The exitance for a given spectral band can be found from the integral of M_e over the bandwidth.

$$M_e = \int_{\lambda_1}^{\lambda_2} M_e(\lambda) d\lambda . \tag{6}$$

Wien's Law gives the spectral location of the peak of the blackbody radiation curve in μm as

$$\lambda = \frac{2898 \mu m \cdot K}{T}, \tag{7}$$

where T is the temperature of the object in Kelvin.

It should be noted that a true blackbody does not exist; it is purely a theoretical concept [21]. A blackbody simulator is the hardware used to provide approximate blackbody output. Nevertheless, many still refer to these as simply blackbodies. For a true blackbody, the total emissivity, ε, is unity. All real sources have a total emissivity less than one, although some blackbody simulators can have total emissivities very close to unity (>0.999). The formula for total emissivity is

$$\varepsilon = \frac{\int_0^{\infty} M_{actual}(\lambda) d\lambda}{M_{total}}, \tag{8}$$

and the formula for spectral emissivity is

$$\varepsilon(\lambda) = \frac{M_{actual}(\lambda)}{M_{blackbody}(\lambda)} . \tag{9}$$

The source radiance may also be used in place of the radiant exitance in these equations.

The emissivity of a non-transmitting material at any given wavelength can be shown to equal unity minus the reflectance of the material at that same wavelength, given that the material is in thermal equilibrium, i.e., its temperature is not changing with time. Thus, good reflectors are poor emitters and vice versa. This is known as Kirchoff's Law. It is Kirchoff who first developed the concept of a blackbody in 1859 [21]. This fact makes cavity-type blackbody simulators very good emitters. Cavities trap incoming light through absorbing multiple reflections and therefore have low reflectivity, and usually have emissivities close to unity. The theory of cavity blackbody simulators will be discussed next.

2.2 Blackbody Simulator Cavity Theory

The goal of any blackbody simulator is to emit radiation that is reproducible, predictable, and close to blackbody radiation. In practice, a blackbody simulator is not difficult to construct. Since good emitters are poor reflectors, a cavity is a very practical shape for a simulator. Cavity-type simulators can produce radiation that is so similar to ideal Planckian radiation, that they can be characterized easily by their deviation from it [22].

Consider a cavity of arbitrary shape constructed out of a conducting material with a small aperture relative to the cavity, as shown in Figure 7. When some amount of radiation is input through the aperture, all but a tiny fraction of the input radiation will be trapped and absorbed.

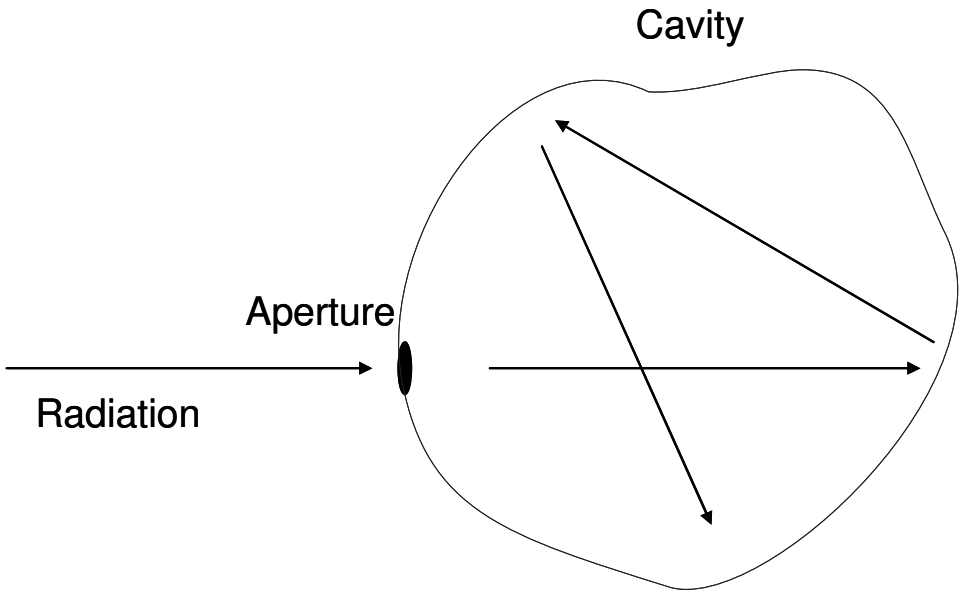


Figure 7. Cavity of Arbitrary Shape

As long as the cavity is in thermal equilibrium, the input radiation will be absorbed only with a small reflected amount exiting back out though the aperture, together with the emitted radiation.

Typical cavity designs that have been used in practice have been spherical, cylindrical, or conical cavities, as shown in Figure 8. Each of these configurations has been studied in detail [23], [24]. Spherical cavities have a more complicated design and are more difficult to construct, but do have better off axis output uniformity. Cylindrical and conical configurations are easier to construct, however, and are suitable for most applications. Reentrant cone designs are another, more complex design. As noted in Chapter I, the reentrant design has been shown to increase the effective emissivity. A reentrant cone cavity configuration is shown in Figure 9.

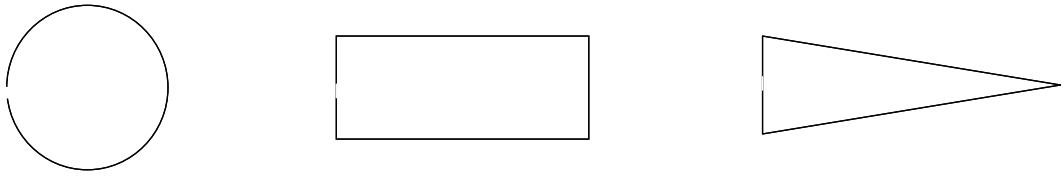


Figure 8. Simple Cavity Configurations

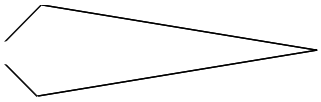


Figure 9. Reentrant Cone Configuration

The derivation of a theoretical expression for effective cavity emissivity is as follows [25], [26]. Consider an isothermal cavity of arbitrary shape constructed with an opaque material with an internal surface area S (which includes the aperture area) and a small aperture, with area s, that is small relative to S. Suppose that a unit of radiation enters the aperture and is incident on the opposite wall and is diffusely reflected according to Lambert's Law. This analysis assumes a perfectly diffuse reflecting surface, the projected solid angle is less than π, and the radiation is uniformly distributed in the cavity after the second reflection. This last assumption means that the cavity surface and aperture areas will not appear in the derivation until after the second reflection. At thermal equilibrium, the incident radiation which is absorbed by the cavity after an infinite number of reflections will be equal to cavity's emitted radiation. A multiple reflection analysis is performed to determine the amount of reflected radiation exiting the aperture and the amount remaining in the cavity. It begins with one reflection and is generalized to an infinite number of reflections.

The fraction of the incoming radiation exiting the aperture after one reflection is

$\rho \cdot F$

where ρ is the diffuse reflection of the material and F is the configuration factor given by

$$F = \pi^{-1} \int_{aperture} d\Omega \quad . \tag{10}$$

The configuration factor is defined as the projected solid angle [20] of the aperture as seen from an arbitrary point on the cavity interior divided by π. Projected solid angle, Ω, is related to solid angle, ω, by

$\Omega = \omega \cos(\theta)$,

where θ is the angle between the aperture surface normal at a given point on the aperture and the line connecting the aperture surface to the cavity surface point. This is illustrated in Figure 10. The projected solid angle must be used since any arbitrary cavity point and the aperture may not be perpendicular to each other.

Thus, after one reflection, the fraction of the radiation,

$1 - \rho \cdot F$

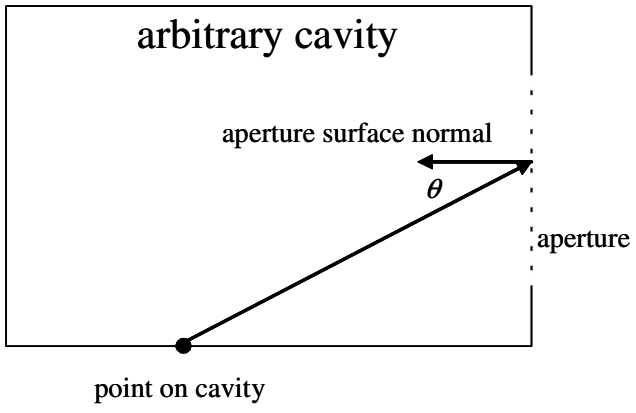


Figure 10. Projected Solid Angle

remains in the cavity. This portion then undergoes a second reflection, where it is again uniformly distributed. The fraction of the twice reflected radiation exiting the aperture is

$$\rho^2(1-F)\cdot\frac{s}{S},$$

leaving

$$\rho^2(1-F)\cdot\left(1-\frac{s}{S}\right)$$

in the cavity, which undergoes a third reflection. After this third reflection, the fraction of radiation exiting the aperture is

$$\rho^3(1-F)\cdot\left(1-\frac{s}{S}\right)\cdot\frac{s}{S},$$

and

$$\rho^3(1-F)\cdot\left(1-\frac{s}{S}\right)^2$$

will remain. Summing over infinite reflections gives the total fraction of reflected radiation, ρ_0, exiting the aperture as

$$\rho_0=\rho\cdot F+\rho^2(1-F)\cdot\frac{s}{S}\left[1+\rho\cdot\left(1-\frac{s}{S}\right)+\rho^2\left(1-\frac{s}{S}\right)^2+\rho^3\left(1-\frac{s}{S}\right)^3+...\right]=\rho\cdot F+\frac{\rho^2(1-F)\frac{s}{S}}{1-\rho\left(1-\frac{s}{S}\right)}. \quad (11)$$

Simplifying, the total effective emissivity of the cavity is given by

$$\varepsilon_0=1-\rho_0=1-\rho\cdot F-\frac{\rho^2(1-F)\frac{s}{S}}{1-\rho\left(1-\frac{s}{S}\right)}=\frac{(1-\rho)\left[1+\rho\left(\frac{s}{S}-F\right)\right]}{1-\rho\left(1-\frac{s}{S}\right)}, \quad (12)$$

and substituting the cavity material surface emissivity, ε, for $1-\rho$ gives

$$\varepsilon_0 = \frac{\varepsilon\left[1+(1-\varepsilon)\left(\frac{s}{S}-F\right)\right]}{\varepsilon\left(1-\frac{s}{S}\right)+\frac{s}{S}}, \tag{13}$$

which is Kelly's formula. Kelly also gives the configuration factor for conical cavities at the apex to be

$$F = \sin^3\left(\frac{\theta}{2}\right) \tag{14}$$

where θ is the cone angle [26]. This equation only applies to conical cavities where the conical base is the aperture.

Kelly's derivation is similar to that of Gouffé [1], [22]. However, Gouffé's analysis contained an error, as noted by Kelly [26] and Bartell [1], [27]. Gouffé's expression for total effective emissivity, ε_0, from a cavity-type blackbody from a back wall location is [1]

$$\varepsilon_0 = \frac{\varepsilon\left[1+(1-\varepsilon)\left(\frac{s}{S}-\frac{\omega}{\pi}\right)\right]}{\varepsilon\left(1-\frac{s}{S}\right)+\frac{s}{S}}, \tag{15}$$

where ω is the solid angle and ε is the total hemispherical emissivity of the cavity material [22]. In the case of the SIRSIII, the back wall is defined as the area of the cavity in the vicinity of the cone apex. Kelly made the correction in Gouffé's analysis by replacing the ω/π term with the configuration factor. Despite Gouffé's error, his method has been reported to predict total emissivities within 1 percent of experimental values [28]. Bartell also notes that Gouffé's expression leads to serious errors when dealing with elongated cavities. Bartell shows that for a conical cavity constructed out of a

material with a total emissivity of 0.5, that Gouffé's theory predicts cavity emissivities that are too low [1].

Gouffé and Kelly both derived their expressions based on multiple reflection analysis. Bartell derived his expressions based on the ratio of radiances and his equation for isothermal cavities can be expressed as

$$\varepsilon_0 = \frac{\varepsilon\left[1+(1-\varepsilon)\left(\overline{F}-F\right)\right]}{\varepsilon\left(1-\overline{F}\right)+\overline{F}} \tag{16}$$

where $\overline{F}$ is the weighted average of the configuration factor F, in its general form as given in Eq. 10. The weighted average of F is a very difficult quantity to calculate. For a first order approximation of Eq. 16, Bartell recommends

$$\varepsilon_0 = 1-(1-\varepsilon)F\,, \tag{17}$$

which does not require the derivation of $\overline{F}$. The derivation of Bartell's method is complicated and can be found in [1]. Bartell and Wolfe [24] give F for a back wall location of a reentrant cone as

$$F = \frac{a^2 \cdot d \cdot (h+l)}{(h+l)^4} \cdot \frac{h+l}{\sqrt{\left(d^2+h^2\right)}}\,, \tag{18}$$

where the variables are defined in Figure 11.

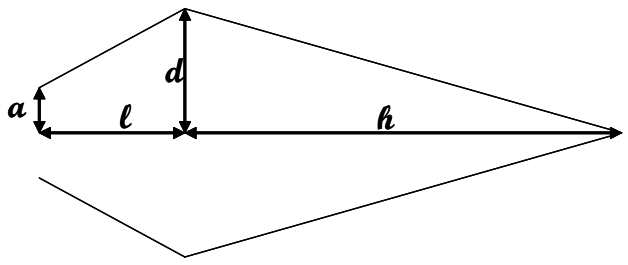


Figure 11. Reentrant Cavity Geometric Definitions

The three theoretical expressions for effective cavity emissivity that have been discussed are summarized in Table 1.

2.3 FTIR Spectrometry Background

As discussed in Chapter I, FTIR spectrometry methods are generally employed in evaluating the spectral emissivity of materials. Experimental setup and instrumentation vary among the users of these methods, but the basic principles of FTIR spectrometry used are the same. Also, use of Kirchoff's Law to measure reflectivity and deduce emissivity is typical. That is, since a direct measurement of emissivity is difficult, most experiments measure the reflectance of the material being measuring and then subtract it from unity to find the emissivity.

Table 1. Theory Summary

Theory	Expression
Gouffé	$\varepsilon_0 = \dfrac{\varepsilon\left[1 + (1-\varepsilon)\left(\dfrac{s}{S} - \dfrac{\omega}{\pi}\right)\right]}{\varepsilon\left(1 - \dfrac{s}{S}\right) + \dfrac{s}{S}}$
Kelly	$\varepsilon_0 = \dfrac{\varepsilon\left[1 + (1-\varepsilon)\left(\dfrac{s}{S} - F\right)\right]}{\varepsilon\left(1 - \dfrac{s}{S}\right) + \dfrac{s}{S}}$
Bartell	$\varepsilon_0 = 1 - (1-\varepsilon)F$

An FTIR Spectrometer uses a Michelson interferometer, as shown in Figure 12 [29], [30]. In these devices, collimated, broad spectral range radiation is input and is incident upon a beam splitter, after which it is incident upon two mirrors, M1 and M2 in Figure 12. One of these is fixed while the other is a moving mirror. In Figure 12, M2 is the moving mirror that creates an optical path difference (OPD) between the two mirrors. A lowercase delta, δ, is used to represent this quantity.

When the two paths are equal, known as zero path difference (ZPD), the waves interfere constructively and give a large intensity signal. The detector records the intensity as a function of the moving mirror position. A Fast Fourier Transform (FFT) is then performed to obtain the intensity as a function of wavenumber, which is the inverse of the wavelength. The Fourier transformation is performed according to

$$I(\upsilon) = \int_{-\infty}^{\infty} I(\delta) \cdot \cos(2 \cdot \pi \cdot \upsilon \cdot \delta) d\delta, \tag{19}$$

where $I(\delta)$ is the intensity as a function of OPD, and υ is the wavenumber.

A Helium-Neon (He-Ne) laser is used to measure the difference in OPD. Since the laser is monochromatic, its interferogram is a sine function, assuming a constant velocity for the moving mirror. The laser detector then can "count" the fringes to measure the mirror position.

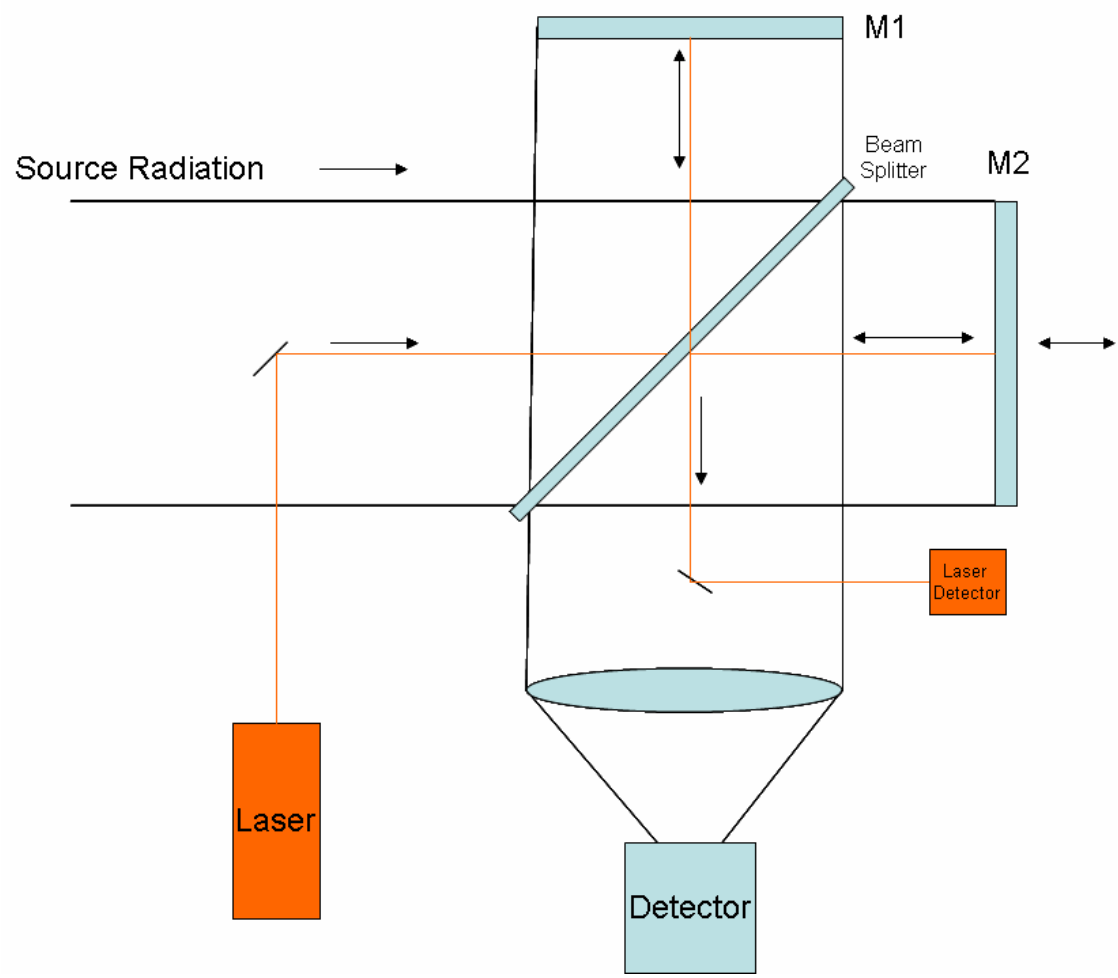


Figure 12. Michelson Interferometer

2.4 AEDC FTIR Instruments

Several laboratories at AEDC have instruments that employ FTIR spectrometry methods. Two different instruments were identified as candidates to make the spectral measurements necessary to determine the emissivity of the SIRSIII blackbody simulator cavity.

The first instrument that was identified is a spectral emissometer, called the Optical Properties Measurement System (OPMS) [12], [31] located in the Aerothermal Measurements Laboratory (ATML). The second instrument, located in the SSTF, is a spectral reflectometer, called the Scatterometer/Reflectometer (SCAT/R). These two instruments were specially made for AEDC by Advanced Fuel Research and A Z Technology, respectively. These instruments will now be described.

2.4.1 Optical Properties Measurement System

The main use of the OPMS, shown in Figure 13, is to measure the spectral emissivity of materials [31]. The instrument has a blackbody simulator source that is modulated through the use of a mechanical chopper located at one focus position of a hemi-ellipsoid mirror (HEM), which redirects the radiation to the other focus position, where the sample to be measured is located.

The mirror has a hole at 15 degrees from the sample normal which allows the radiation that reflects and emits from the sample to enter an optical system that directs it into the FTIR Spectrometer. A schematic of the instrument is shown in Figure 14. The OPMS uses a Mercury-Cadmium-Telluride (MCT) detector that outputs a voltage signal that is sent to an analog-to-digital converter (ADC) where the signal is digitized.



Figure 13. Optical Property Measurement System

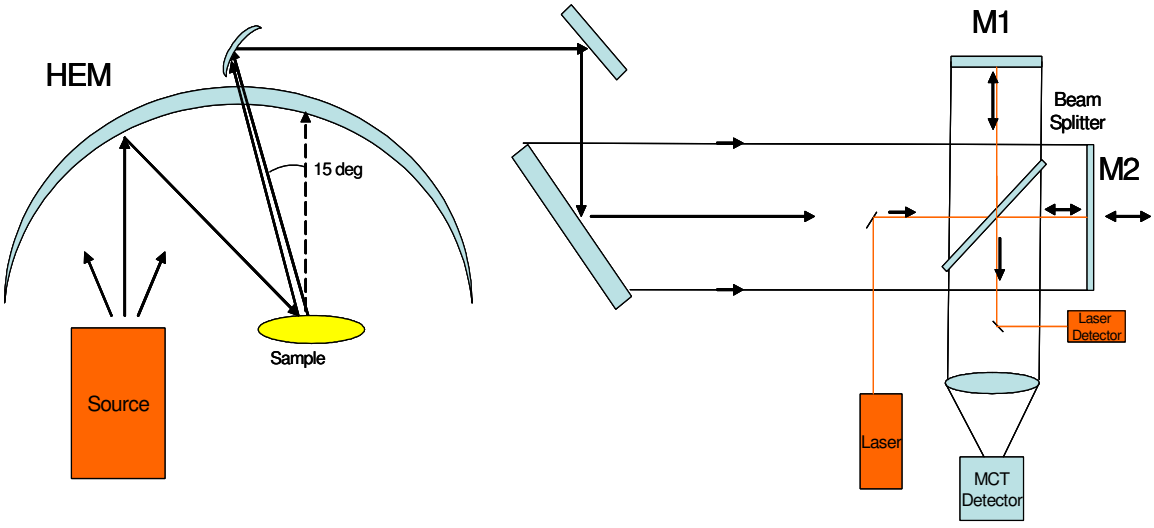


Figure 14. OPMS Schematic

The MCT detector has a responsive range of 1.6 to 20 μm and is operated at a temperature of 77 K through the use of liquid Nitrogen (LN_2). The instrument software performs all the required manipulation of the data, transforming the interferograms to spectra, converting the wavenumbers (cm^{-1}) to microns (μm), and calculating the spectral emissivity from the spectral reflectivity.

The source is operated at 800° C (1073.15 K), and is controlled to within 2° C. Below 1.25 μm, there is not sufficient energy from the blackbody simulator to obtain a good signal to noise ratio on the reflected radiance from samples [12].

The measurement process will now be described. First, the combined sample radiance and reflected source radiance are measured, and this total quantity is denoted as $M_1(\upsilon)$. This measured quantity is described by the equation

$$M_1(\upsilon) = L_s(\upsilon) + \rho_s(\upsilon) \cdot L_{BB}(\upsilon), \tag{20}$$

where $L_s(\upsilon)$ is the sample radiance, $\rho_s(\upsilon)$ is the sample reflectance, and $L_{BB}(\upsilon)$ is the OPMS source blackbody simulator radiance. The OPMS source is then blocked with the chopper in order that the sample radiance can be measured, which is the first term of $M_1(\upsilon)$. This second measurement is then

$$M_2(\upsilon) = L_s(\upsilon). \tag{21}$$

The amount of the source radiance reflected by the sample can be then determined by subtracting the two measurements, leaving

$$M_1(\upsilon) - M_2(\upsilon) = M_3(\upsilon) = \rho_s(\upsilon) \cdot L_{BB}(\upsilon). \tag{22}$$

In the calibration, a gold mirror is placed in the sample position and a reference measurement. Gold has very high reflectance in the infrared and in the data processing

routines, the OPMS manufacturer input its spectral reflectivity to be unity. This reference measurement is

$$M_{ref}(\upsilon) = \rho_{gold}(\upsilon) \cdot L_{BB}(\upsilon). \tag{23}$$

The right-hand side of Eq. 22 is divided by the right-hand side of Eq. 23, which leaves the ratio of the spectral reflectivities,

$$\frac{\rho_s(\upsilon)}{\rho_{gold}(\upsilon)}, \tag{24}$$

where $\rho_{gold}(\upsilon)$ is assumed to be unity, leaving only the sample reflectance. Emissivity is then calculated according to Kirchoff's Law. Figure 15 shows a flow diagram of the measurement process.

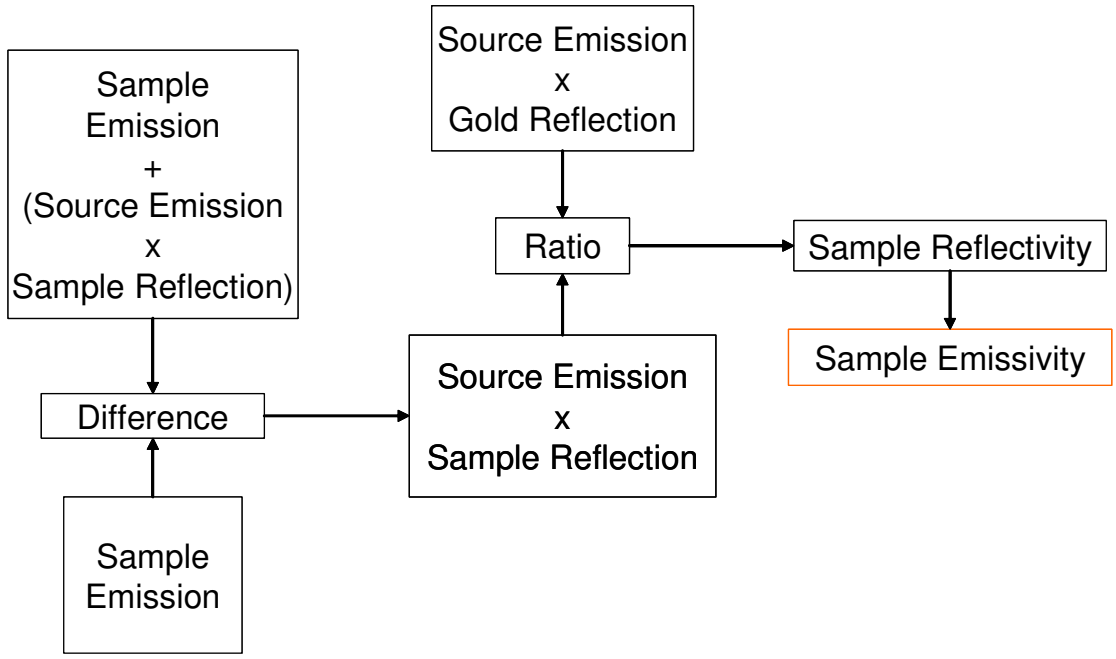


Figure 15. OPMS Measurement Process

2.4.2 Scatterometer/Reflectometer

The second instrument used, the SCAT/R, shown in Figure 16, is designed to measure optical surface finish scattering characteristics. The SCAT/R can measure spectral scatter and reflectance from 2.5 to 15 μm at five different angles of incidence (15°, 30°, 45°, 60°, 75°) as defined from the surface normal.

In the full measurement mode, the instrument makes the following measurements: total, specular, diffuse, and retro reflection, total integrated scatter (TIS), and root-mean-square (RMS) surface roughness. The total, specular, and retro reflection measurements are made directly. Diffuse reflectance is calculated by subtracting the specular from the total reflectance. The fundamental operating principles of the SCAT/R are similar to the OPMS as it also has a FTIR spectrometer. The beam from an internal interferometer is focused at the port on top of the instrument to measure the reflectance of samples. The detectors used for the various types of measurements are shown in Table 2.



Figure 16. SCAT/R Instrument

Table 2. SCAT/R Detectors

Measurement	Detector	Operating Temperature
Incident Power	Deuterated Triglycine Sulfate	Room, ~300 K
Specular Reflectance	Mercury Cadmium Telluride	77 K
Retro-reflectance	Mercury Cadmium Telluride	77 K
Total Reflectance	Pyroelectric	Room, ~300 K

A schematic of the SCAT/R is shown in Figure 17. The focusing and collecting optics are greatly simplified in order to show the general operating principle of the instrument. The instrument is calibrated using a gold reflectance standard. When the instrument was initially constructed, the gold standard reflectance values were input into the calibration software. When the instrument is calibrated using the same standard before a measurement, the software calculates the ratio of the detected signal to the initial calibration.

When a measurement sample is put into position, the changes in detector signal from the calibration are directly correlated to the deviation of the sample's reflection from that of the standard. And thus, the absolute reflection of the sample is measured.

A more detailed overview of the instrument will now be given [32]. The source used is a ceramic igniter (typically used in gas and combustion applications) and operates at a temperature of approximately 1550 K. An off-axis parabolic (OAP) mirror collects a 1.5 mm^2 area of the source and collimates the radiation, which is then input into the interferometer. The collimated beam exits the interferometer where another OAP mirror reflects the beam toward the sample plane.

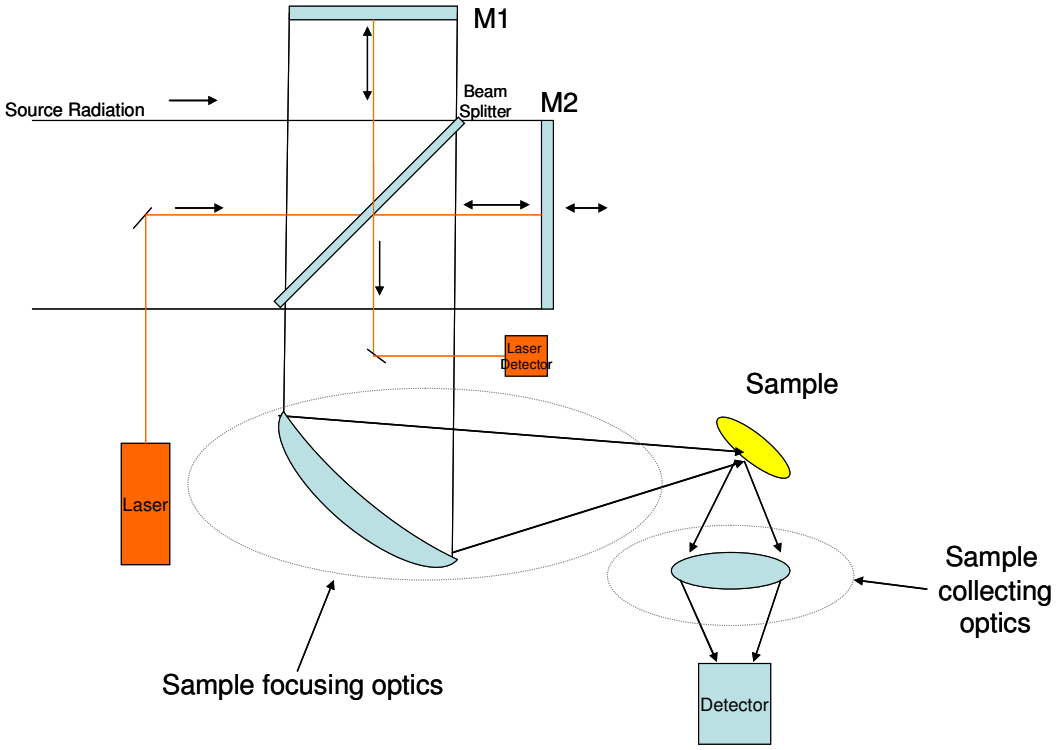


Figure 17. SCAT/R Schematic

After reflecting off the second OAP mirror, the beam passes through a 2-mm field stop and then is incident on a silicon beam splitter. The transmitted portion of the beam is then reflected off a fold mirror, located on a mirror stage powered by a Geneva drive. A fold mirror is a flat mirror that changes the direction of the incident radiation. There are five mirror stages, each with a fold mirror, each one corresponding to an angle of incidence (AOI). The beam is reflected off this fold mirror to the corresponding spherical mirror, which focuses the beam onto the sample. The manner in which the reflected beam(s) is captured is dependent on the measurement being performed.

The total hemispherical reflectance measurement uses ellipsoidal collector technology. This collector is positioned with a translation stage that can repeat placing

the ellipsoid on the measurement location to within 0.0005 inches. The ellipsoid has five apertures, each corresponding to an AOI. The radiation from the spherical mirrors is focused onto the sample through the corresponding aperture. The ellipsoid is positioned so that the sample is at one focus. The ellipsoid collects the radiation at the second focal point where a pyroelectric detector resides.

The ellipsoid is not used in specular reflection measurements. The collection of the specularly reflected beam for measurement is as follows. Each stage of the Geneva drive has two mirrors. The first mirror folds the beam to the appropriate spherical mirror that focuses the beam onto the sample. The reflected beam is then collected by another spherical mirror that sends the beam to the second fold mirror on the mirror stage, which reflects the beam to the MCT detector used for specular reflectance measurements. The second spherical mirror configuration for the collection of specular reflectance is identical to the input mirror configuration. The system is designed so that the detector's field of view minimizes the collection of spurious radiation.

2.5 Summary

This chapter described the basic fundamental theory of blackbody radiation and then applied that to blackbody simulator cavities. Three theoretical expressions for the effective emissivity of a blackbody simulator were described. Next, FTIR Spectrometers were described, as they were identified as a way to measure the spectral emissivity of the SIRSIII cavity. Two FTIR based instruments were also described that were identified to perform the measurements. The methodology and procedures used in applying the theories and experimental equipment will now be discussed in Chapter III.

CHAPTER III

METHODS FOR DETERMINING SPECTRAL EMISSIVITY

The previous chapter described the theoretical and experimental background of this research. This chapter illustrates the application of that background information to the SIRSIII blackbody simulator cavity.

3.1 Theoretical Methods

The SIRSIII cavity is constructed from black anodized aluminum. The spectral emissivity of anodized aluminum has previously been measured at AEDC using the OPMS and this data was obtained for use in this research [33]. Figure 18 shows this data taken for the material at a temperature of 300 K. The spectral resolution, or the smallest spectral features that the instrument can distinguish, of the data is 32 cm^{-1}.

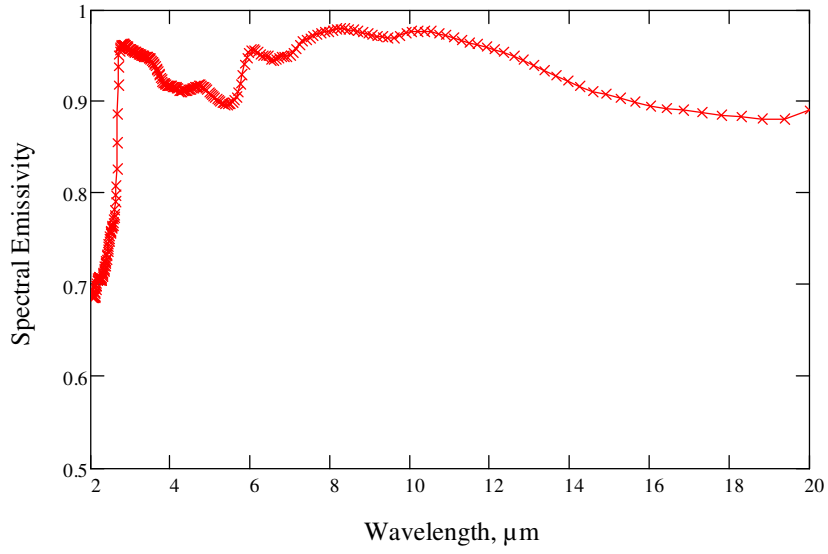


Figure 18. Anodized Aluminum Hemispherical Spectral Emissivity

Although the resolution is given in wavenumbers, the data is shown in wavelength with units of μm. This is why when the data is displayed in wavelength, the number of data points decreases with increasing wavelength. Anodized aluminum has very good emissivity, remaining above 0.85 from approximately 3 μm out into the far IR. It was assumed that this data represents the "true" value of the emissivity, i.e., there is no uncertainty.

The cavity and aperture surface areas were calculated using simple geometric formulas for cones. With the reentrant cap, the surface area of the cavity is 1.387 in^2, and without the cap, the surface area is 1.322 in^2. The anodized aluminum spectral emissivity data was input as the material spectral emissivity into the theoretical equations. From these inputs, a resultant effective cavity spectral emissivity for the SIRSIII was calculated. These calculations were performed for a back wall location. It was assumed that the anodized aluminum data used was typical for this material and is representative of the SIRSIII anodized aluminum. This is not a bad assumption, since the anodization process was the same for both. It was also assumed that the emissivity does not vary significantly with temperatures within ±10 K of 300 K. The calculations were carried out for the SIRSIII with and without the reentrant cap. In the calculations with the reentrant cap, Eq. 18 was used to calculate the configuration factor, F, and resulted in a value of 7.99×10^{-4}. Without the reentrant cap, the SIRSIII becomes a conical cavity where the conical base is the aperture. Eq. 14 gave the F for this configuration to be 3.828×10^{-3}, which was used in the calculations.

All the theoretical calculations were performed in Mathcad 13® [34]. This software allows the user to type mathematical expressions just as they would appear on

paper. It has a multitude of built in functions for mathematical operations and also allows users to define or create their own functions. A programming toolbar also allows programs to be written. External data can be imported for use in the software through a file input function. This software was chosen for these reasons and for its straightforwardness in performing complex mathematical computations. The anodized aluminum emissivity data in Excel® format was input into Mathcad® through the file input function. The data was linearly interpolated to give a spectral resolution of 0.1 μm using Mathcad's® linterp function. The theoretical equations of Gouffé, Kelly, and Bartell as given in Eqs. 15, 13, and 17, respectively, were entered and the results were then calculated based on the input anodized aluminum data.

The literature uses these methods as formulae for computing total emissivity. In this analysis, they were used to calculate spectral emissivity. To calculate the effective total emissivity of a cavity, the total emissivity of the cavity material would be input into the theoretical equations of Gouffé, Kelly, and Bartell. In this thesis, the spectral emissivity of the cavity material was input into these equations. To validate the use of the theories in this manner, first, the total emissivity of anodized aluminum, 0.923 in the 2 to 20 μm range, was input into the theoretical equations to find the SIRSIII effective total emissivity. Next, the anodized aluminum spectral emissivity data was input into the theoretical equations to find a resultant SIRSIII effective spectral emissivity. This resultant effective emissivity was then used to calculate an effective total emissivity for the SIRSIII according to the equation

$$\varepsilon_t = \frac{\int_2^{20} \varepsilon_\lambda(\lambda) \cdot L_e(\lambda) d\lambda}{\int_2^{20} L_e(\lambda) d\lambda}, \tag{25}$$

where $L_e(\lambda)$ is the spectral radiance of the SIRSIII at a temperature of 300 K. Figure 19 shows a flow diagram of the calculation process. The results of these differing methods to calculate the cavity total emissivity are shown in Table 3. The notations ε_t and ε_λ refer to the total and spectral emissivity respectively. The total emissivity results are virtually identical, with percent differences being equal to or less than 0.004%. These miniscule errors are most likely due to the computational algorithms in Mathcad® used to find the values.

Although the Standard Source is always used in the 7V Chamber with the reentrant cap in place, the calculations were also performed with the s/S and F values that represent the reentrant cap off to examine the cap's effect on the effective cavity spectral and total emissivity, and to compare them with the experimental work described below.

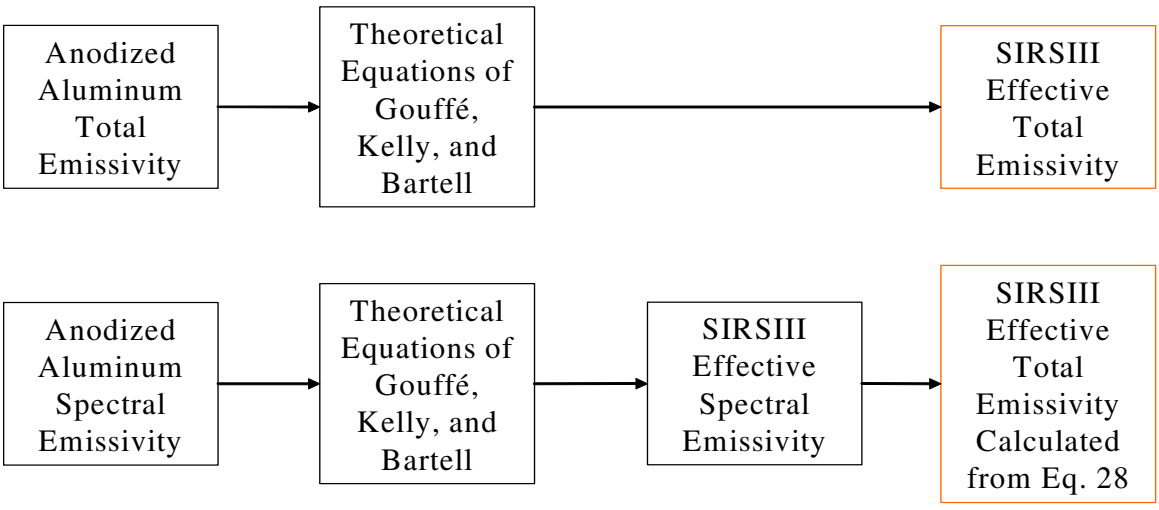


Figure 19. SIRSIII Total Emissivity Calculation Process

Table 3. Comparison of Total Emissivities

Method	ε_t derived From ε_λ	ε_t	Percent Difference
Gouffé	0.99942	0.99938	0.004
Kelly	0.99972	0.99972	0.000
Bartell	0.99994	0.99993	0.001

The calculations without the reentrant cap cannot be compared to any data taken with the Standard Source in the 7V Chamber, but they do show how the total and spectral emissivities change with aperture size and configuration factor, and thus provide another comparison between the theory and measurements performed.

3.2 OPMS Measurement Method

As noted previously, the OPMS spectral scans were done in an AEDC laboratory. Several steps were taken prior to the SIRSIII measurements to ensure the stable and reliable operation of the OPMS. First, the instrument was allowed to warm up for approximately two hours. This ensured the source and interferometer were in a stable operating condition. Also, the MCT detector dewar in the spectrometer was filled with liquid nitrogen (LN_2) to ensure optimal performance. After the instrument had warmed up, an instrument calibration was performed using a gold reference mirror. This calibration also serves as the reference measurement in Eq. 23. The calibration was then verified using a painted reference sample known as “1614”, because it has a well-known spectral emissivity. It was desired to perform the OPMS measurements with the SIRSIII cavity held at a constant temperature as close to 300 K as possible to correlate them with the anodized aluminum emissivity data. A thermocouple was inserted behind the cavity

to monitor its temperature, and display it on a thermocouple readout device. The temperature was measured and manually recorded just prior to each measurement run.

To begin the measurements, the SIRSIII cavity was placed in a vise at the measurement position. The cavity was then aligned so that the three alignment lasers intersected at the cavity aperture. Five spectral scans were performed with the reentrant cap in place. Without disturbing the cavity position, the reentrant cap was removed. Then, five spectral scans were performed without the reentrant cap. The heat from the OPMS source was blocked using its chopper in between each measurement run so that the SIRSIII cavity temperature remained below 310 K.

The software used in the OPMS data acquisition and analysis is Spectra Calc® [35], which is written in Array Basic® (AB). This software is supplied by the instrument manufacturer. In Spectra Calc, an AB program called "BT" is run to collect the data. Another AB program called "BTCOMP" is used to process the data. "BTCOMP" takes the raw data in the form of voltages and computes the spectral emissivity at each sample wavelength, in microns. The results of the measurements are stored in .spc files which are converted to .prn files using a QBasic program called SPECX1. The .prn files can then be imported into other software programs for plotting and further analysis. In this case, the .prn files were input into Excel® on the ATML laboratory computer and then brought back to the author's office computer and input into Mathcad® in the same manner as previously described for the theoretical calculations.

The OPMS is set up to measure a hemispherical spectral emissivity at 15^{o} from the sample surface normal. Since hemispherical spectral emissivities are measured, the measurements are the same as the normal emissivities needed for the theoretical

calculations, which were performed for a normal emissivity at the apex of the cavity cone due to the deep SIRSIII cavity. It was desired to perform the theoretical calculations at the cone apex since it greatly simplifies the calculation.

3.3 SCAT/R Measurement Method

The SCAT/R instrument is designed to measure total hemispherical spectral reflectivities of material surfaces where the sample surface is located at a measurement port. It was not known beforehand how the instrument would perform when a cavity would be located at the measurement port. The specular reflection method must have the output beam reflect off the sample at one of the five fixed angles. Past experience with the instrument has shown that the retro-reflection from highly reflecting samples is low and would be virtually zero for a diffuse cavity. Therefore, these measurements would not be suitable to determine the SIRSIII cavity reflectivities. However, it was believed that by making the measurements in total hemispherical reflection mode, these issues could be overcome. The hemi-ellipsoidal collector makes a total measurement by collecting all the radiation over 2π steradians, allowing it to collect all the scattered and reflected radiation from the cavity.

The instrument has five available input beam angles to choose from. At the smaller vertical angles (15^o and 30^o), the beam diameter is on the order of 3 mm. At the larger angles of incidence, the spot elongates and is no longer circular. Past experience has also shown that measurements made with the incident beam at 15^o are very repeatable. For these reasons, it was decided to make all the measurements on the SIRSIII cavity with an incident beam angle of 15^o.

The MIDAC Corporation manufactured the interferometer used in the SCAT/R and supplied it with the GRAMS/32® [36] software to operate it. The SCAT/R software is the operating software for the entire instrument. GRAMS/32® is designed for data processing and handling, and is typically used in spectroscopic applications. It also provides an operating environment to call and execute specific AB programs. A program written specifically for the SCAT/R by the manufacturer called "SCATR.AB" is the measurement program and was used to perform these measurements.

After the OPMS measurements, the thermocouple was left inside the cavity so it could be used in the SCAT/R measurements. A handheld thermocouple reader was used to read the temperature. The cavity was allowed to reach equilibrium with the room temperature before the measurements were performed and the temperature finally stabilized at 302 K. The temperature never deviated more than ±1 K during the course of the measurements.

To begin the measurement process, a total reflectivity calibration was made using the gold reflectance standard. To account for any background signal that was not accounted for in the calibration, five reflectivity scans over the wavelength interval were performed with an open port (no sample). The average of the background scans is shown in Figure 20. In the data reduction, the average of these baseline scans was subtracted from the measurement data.

Next, the SIRSIII cavity was placed at the measurement port position. The cavity aperture and the ellipsoidal collector were visually aligned. In the SCATR.AB graphical user interface (GUI), the "User Selects Mode" was chosen in the mode such that only total reflectance measurements were performed at each wavelength.

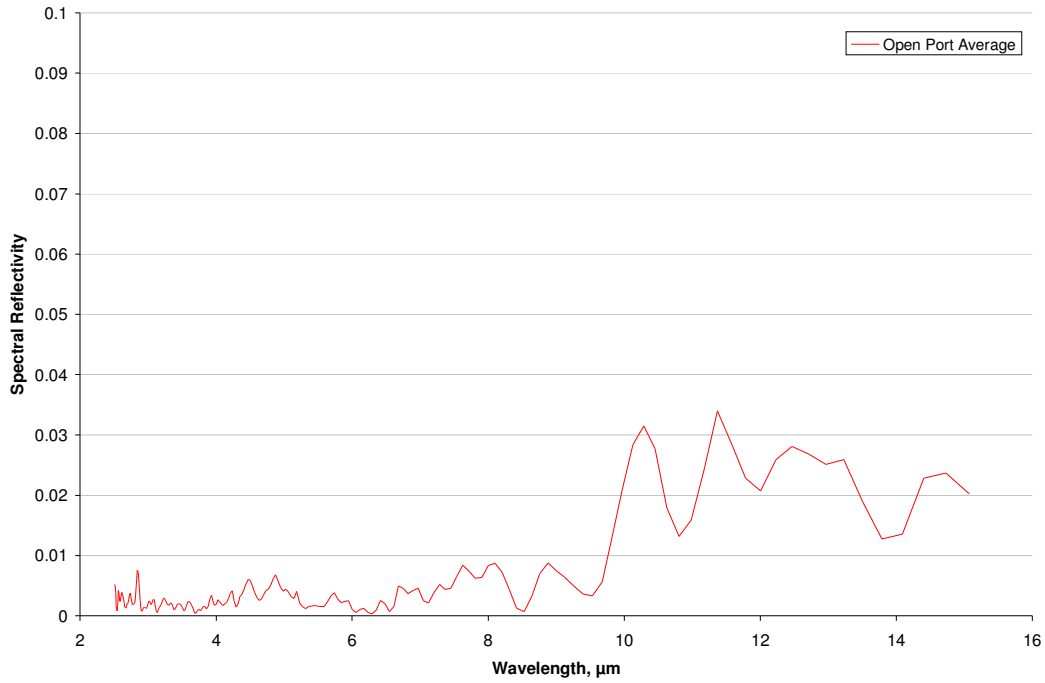


Figure 20. Averaged Spectral Reflectivity for Open Port on SCAT/R

The measurement parameters of total reflection incident beam at 15^{o} were also selected in the software. The default spectral resolution is 32 cm^{-1} and this was not changed. Five total reflection scans over the wavelength interval were performed, with and without the reentrant cap in place.

The reflectance data was automatically saved by the program in .spc format and then converted to a .txt file through the export command in GRAMS/32®. The SCATR.AB program automatically converted the reflectance data to a function of wavelength, in microns. The data was then imported into Excel® and from Kirchoff's Law, the hemispherical spectral emissivity distribution was calculated, after which the data was imported into Mathcad® for plotting and further analysis.

3.4 Uncertainty Analysis Method

After the data was taken, an uncertainty analysis was performed. The uncertainty analysis methodology used is in accordance with NIST methods [37]. These methods are based upon the *Guide to the Expression of Uncertainty in Measurement* published by the International Organization for Standardization (ISO) [38]. The NIST methods classify uncertainty into two categories, Type A and Type B. Type A uncertainty is derived by statistical methods, such as calculating standard deviations of the data, and Type B uncertainty is evaluated by more heuristic means. Type B analysis relies on scientific judgment, previous measurements, knowledge about the measurement systems, instrument specifications, etc.

The analyses were performed in Excel® to utilize its error bar plotting capabilities. With only five data sets, the actual distribution of error in the data was unknown. Therefore, normal (Gaussian) distributions of error were assumed to hold for Type A uncertainties, which were calculated as the standard deviation of the data, according to the equation

$$\sigma = \sqrt{\frac{\sum (x - \bar{x})^2}{(n-1)}}, \tag{26}$$

where x is the data point, $\bar{x}$, is the mean of the data set, and n is the number of data points. The standard deviations were calculated at each wavelength for the five spectral scans.

For Type B uncertainties, an analysis was performed for each instrument that identified possible sources of this uncertainty type. Information was gathered from

published literature, calibrations, and manufacturer documentation. Specific Type B uncertainty values or sources for the OPMS and SCAT/R are given below.

The Type A and Type B uncertainty values were combined using the root-sum-square (RSS) method to find combined standard uncertainty values in the reported emissivity data. An expanded uncertainty was found by multiplying the combined standard uncertainty values by a coverage factor, k=2, to give a 95% confidence interval.

For the OPMS, Type A uncertainties were expected to be small, with systematic uncertainties, Type B, contributing the most to overall uncertainty, due to the time it takes the instrument to make a measurement, which is approximately 8 seconds [39]. The most significant source of Type A uncertainty was expected to be instrument electrical noise in the detector output signal. The same was expected for the SCAT/R measurements; however, previous experience has shown that the Type A uncertainties can be significant for this device.

Several possible sources of Type B uncertainty were identified for the OPMS. The calibration sample for the OPMS is a gold reference mirror. In the emissivity calculation performed by the software, its reflectance is taken to be 100%. In reality, the spectral reflectance of gold from 2-20 μm ranges from 98.5 to 99.5% [40]. There will also be a small amount of radiation loss due to the mirror hole. This radiation will be emitted from the OPMS source through the hole without ever being incident on the sample being measured. Previous analysis performed by Wood, et. al. calculated the loss to be 1.78% of the total energy [41]. Another possible source is related to the OPMS source temperature, which has a random uncertainty of $\pm 2^{o}$ C [39]. This results in a 0.29 W/cm^2 uncertainty in its radiant exitance. In between measurements, if the temperature

of the source fluctuated, it would result in a bias in the measured emissivity. The last possible identified source was instrument calibration quality. A well-known reference sample was used to verify the instrument calibration, by taking three reference measurements using the 1614 painted reference sample. This data was analyzed to determine if any calibration bias was present.

For the SCAT/R instrument, only two possible sources of significant Type B uncertainty were identified. The first uncertainty source is attributed to the ellipsoid collector. The collector has 5 entrance holes through which incident radiation is projected onto the sample. A small amount of radiation will be lost through these holes after being reflected off the sample. The manufacturer states the loss per hole to be 0.0075% of the total reflected beam, and with five holes the total loss is 0.0375%. This hole loss results in a lower measured reflectance, and thus a higher calculated emissivity. The second uncertainty source consisted of any biases in the instrument calibration. The manufacturer has previously determined a calibration Type B uncertainty.

3.5 Relation of Measurements to 7V Standard Source

After the analysis of the measurement data, the results were applied to predict the uncertainty level in the radiometric output of the Standard Source in the 7V Chamber. In this analysis, only the case with the reentrant cap was considered, as the Standard Source is always used with it in place. The Standard Source effective radiance is the quantity measured during the 7V CMS detector calibration and it is calculated according to

$$L_{eff} = \frac{1}{\pi}\int_{2}^{30} R_N(\lambda) \cdot \frac{3.74\times10^4}{\lambda^5 \cdot \left(e^{\left(\frac{14388}{\lambda T}\right)} - 1 \right)} d\lambda \,, \tag{27}$$

where $R_N(\lambda)$ is the known normalized Si:As detector response. The effective spectral radiance is simply the integrand in Eq. 27.

Mathcad® was once again used to perform the calculations. For the OPMS and SCAT/R measurement data, the averaged data were used to calculate the effective spectral radiance. The lower and upper bounds for the measured emissivity was also used to calculate this quantity. These bounds are derived from the expanded combined uncertainty calculated for each measurement set. All the calculations in this analysis were performed for the Standard Source at a temperature of 302.9 K to check the results against Standard Source data obtained at that temperature.

CHAPTER IV

THEORETICAL AND EXPERIMENTAL RESULTS

This chapter describes the results of the theoretical calculations and the measurements obtained with the OPMS and SCAT/R instruments. Extensive data analysis and application of the results to the 7V Chamber Standard Source are presented.

4.1 Theoretical Results

The results of the theoretical calculations with the reentrant cap on and off are shown in Figures 21 and 22, respectively. Gouffé's theory predicts the lowest emissivity, with Kelly's in the middle, and finally the Bartell approximation predicts the highest emissivity. The reentrant cap increases the effective emissivity due to the fact that the reentrant cap results in a lower value for the configuration factor, F. The cap also decreases the aperture size while increasing the cavity surface area.

4.2 OPMS Measurements

4.2.1 Results

The results of the OPMS measurements of cavity spectral emissivity will now be discussed. Over the course of the five measurement scans over the wavelength range, the temperature of the cavity ranged from 302 to 310 K for each scan. This is not a significant temperature difference and it had virtually no effect on the measured emissivities, which is apparent from the data. Figure 23 shows the five measurements with the reentrant cap on and Figure 24 shows the average of the data.

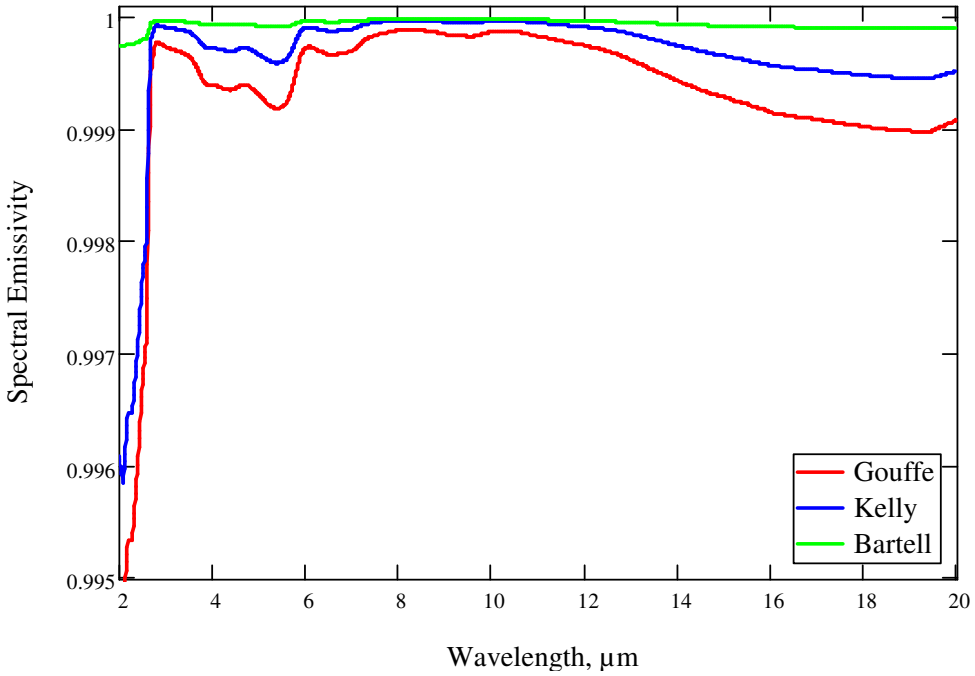


Figure 21. Theoretical Spectral Emissivity with Reentrant Cap

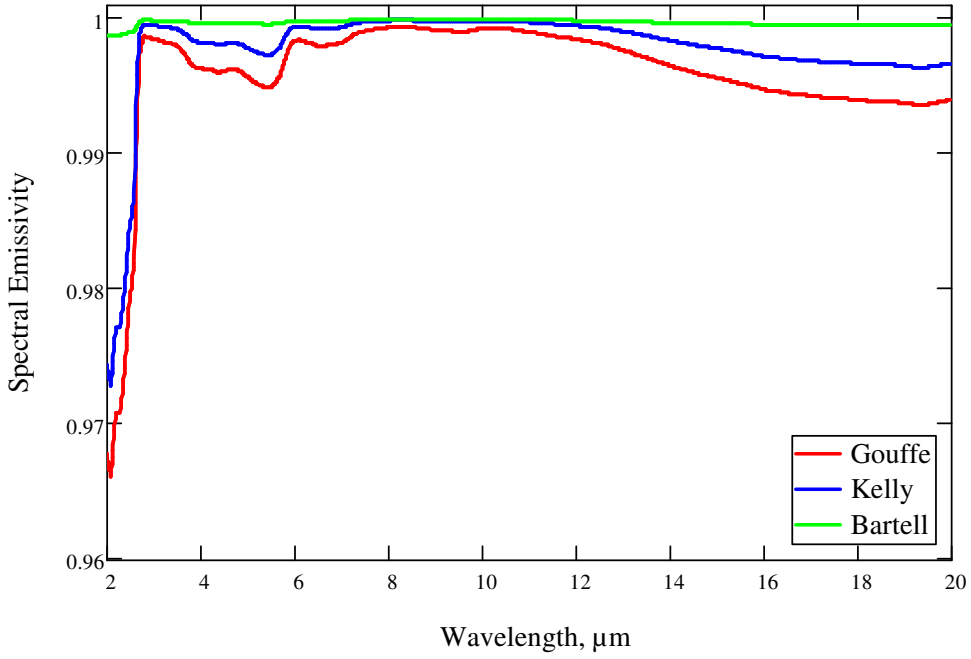


Figure 22. Theoretical Spectral Emissivity without Reentrant Cap

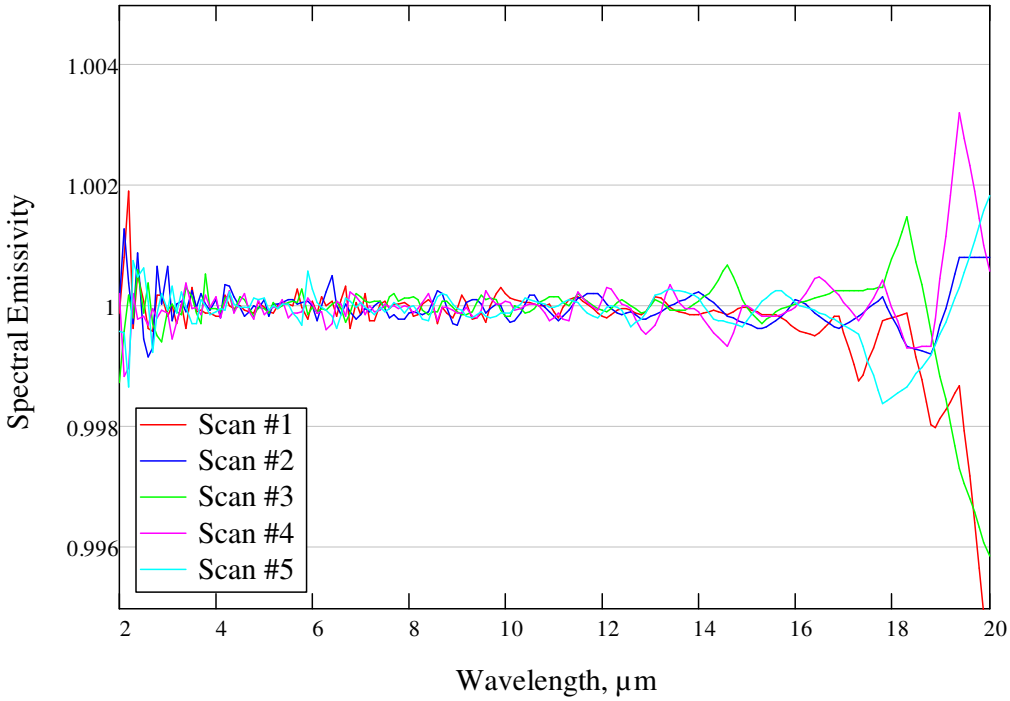


Figure 23. OPMS Measured Spectral Emissivity with Reentrant Cap On

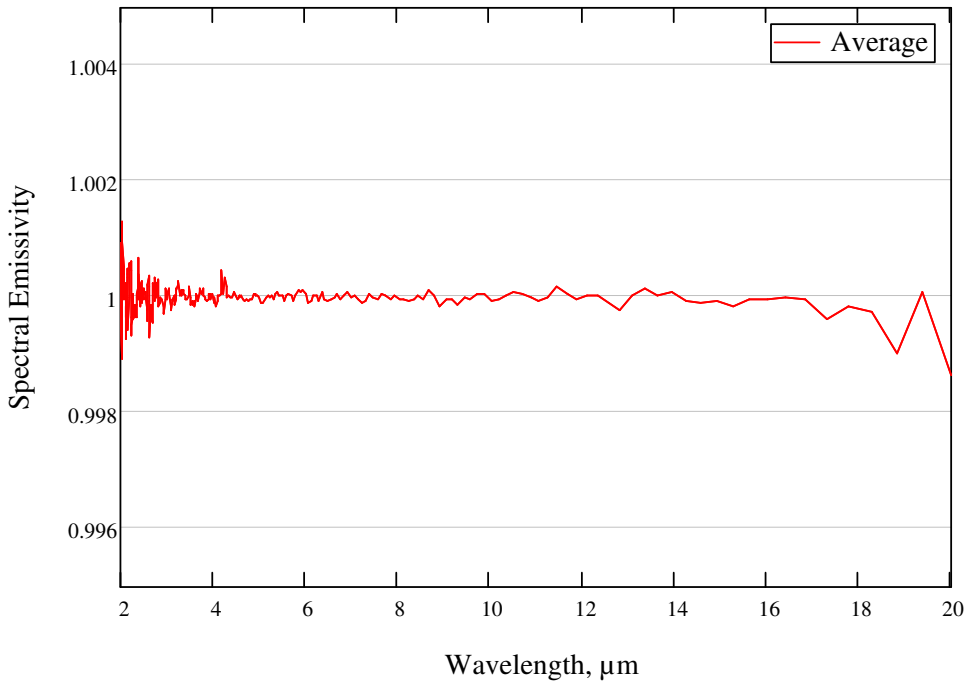


Figure 24. OPMS Average Measured Spectral Emissivity with Reentrant Cap On

Very little noise is present in the data except in the region below 4 µm and beyond 16 µm. The high absorption of the cavity caused very little radiation to be reflected, giving an experimental spectral emissivity of basically unity over the 4 to 16 µm range. Some of the measured values are slightly greater than one. Since this is physically impossible, it is attributed to instrument noise, which is demonstrated when the apparent noise decreases for averaged data.

The results of the five OPMS measurements with the reentrant cap off are shown in Figure 25. The region beyond 16 µm exhibits similar noise to the measurements with the reentrant cap in place. The reentrant cap caused an undetectable amount of radiation to be reflected off the core in the previous measurements; however, there was enough reflected radiation in the 2 to 6 µm range off of the core without the reentrant cap to see more structure in the spectral emissivity data curves.

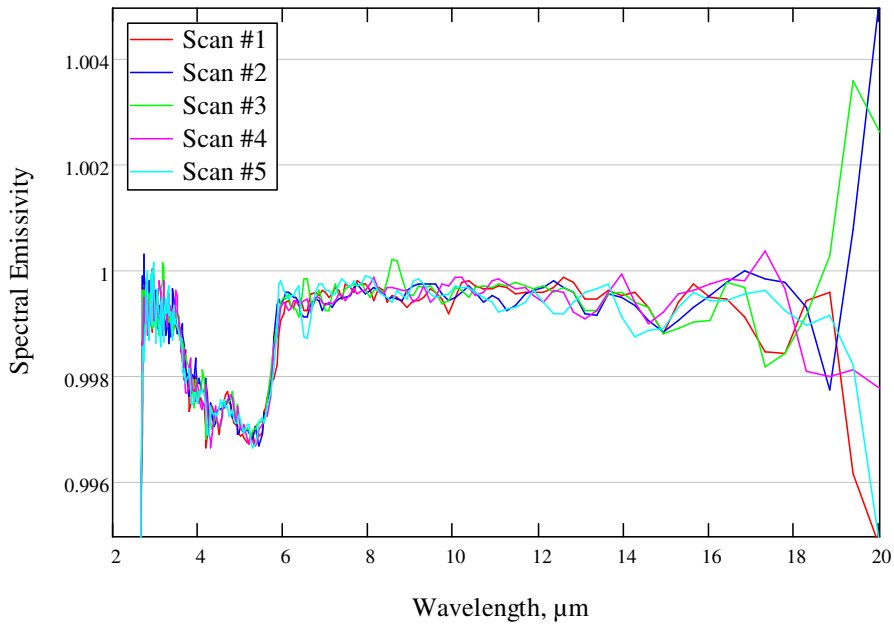


Figure 25. OPMS Measured Spectral Emissivity with Reentrant Cap Off

Once again, noise causes some values to rise above one, and this is attributed to instrument noise. When the data is averaged, all the data points fall below unity. Figure 26 shows the average of the five data runs. The data runs also exhibit excellent repeatability.

4.2.2 OPMS Data Uncertainty Analysis

The results of the uncertainty analysis performed on the OPMS data will now be discussed. For the Type A uncertainty, the maximum standard deviations in spectral emissivity over all five scans with and without the reentrant cap were 3.42 x 10^{-3} and 4.70 x 10^{-3}, respectively. These values occur at the final data point recorded at 20 µm, where the most noise was seen.

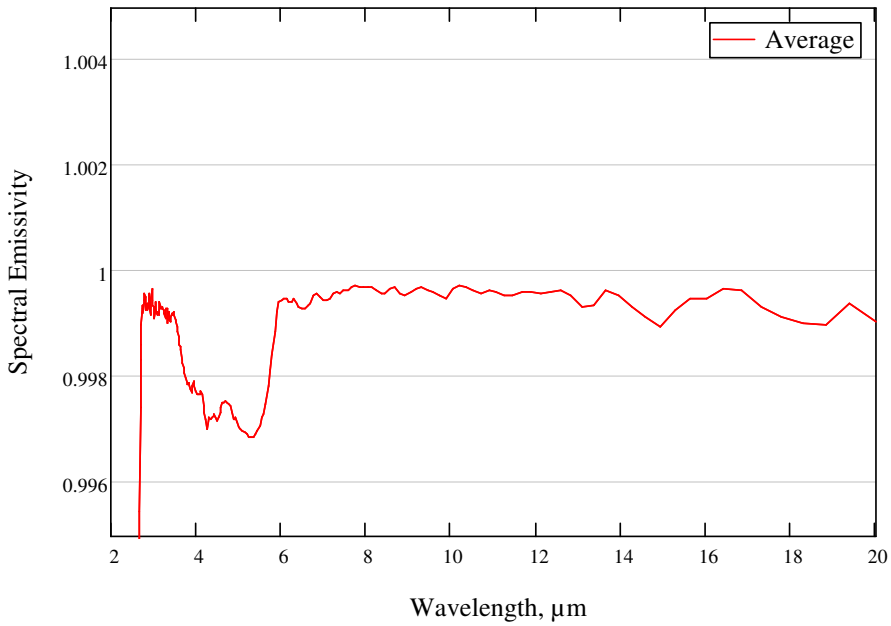


Figure 26. OPMS Average Measured Spectral Emissivity with Reentrant Cap Off

This is not surprising given that there is little energy being emitted from the instrument source at the longer wavelengths, and thus less energy incident on the SIRSIII cavity, which is also emitting very little energy this far into the infrared, given that its temperature stayed at about room temperature. The cavity's peak emission was calculated to be at 9.3 µm according to Wien's Law. The particular spectral response for the OPMS MCT detector is not known, but typically the responsivity of these detectors drops significantly after approximately 13 µm. Knowing these factors, it is reasonable that measurement noise was larger at the lower and longer wavelengths. A good estimation of the best data range with the least noise would be approximately 3 to 16 µm. This can be more clearly seen in the data with the reentrant cap on, as more noise is seen at the beginning and end of the spectra. Figures 27 and 28 show the Type A uncertainty plotted with the mean for the cases with the reentrant cap on and off respectively.

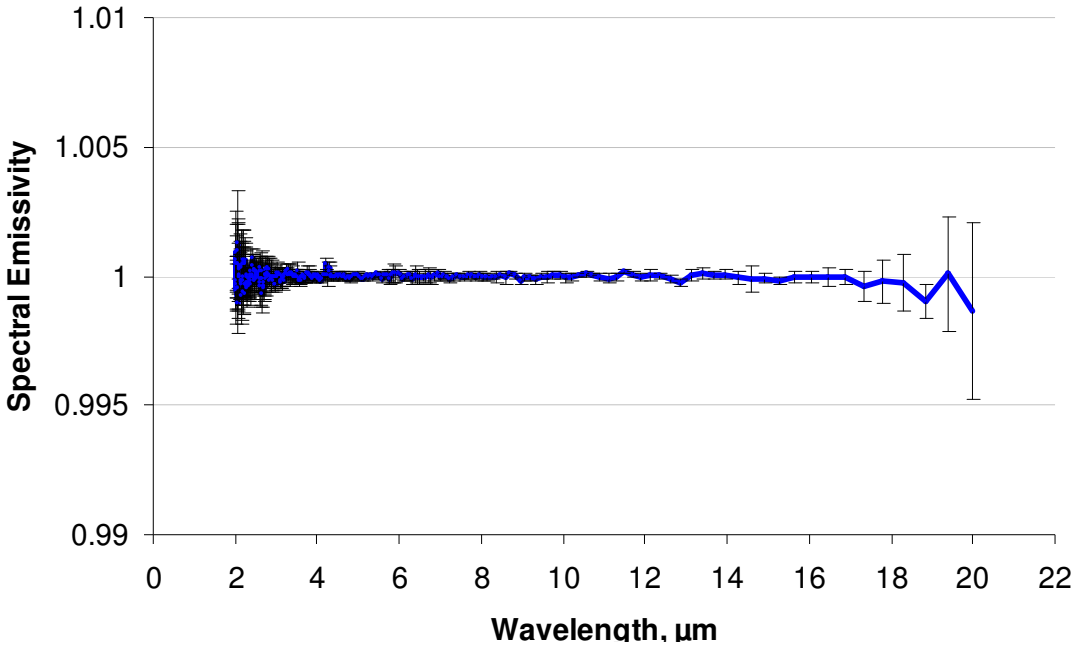


Figure 27. OPMS Type A Uncertainty – Cap On

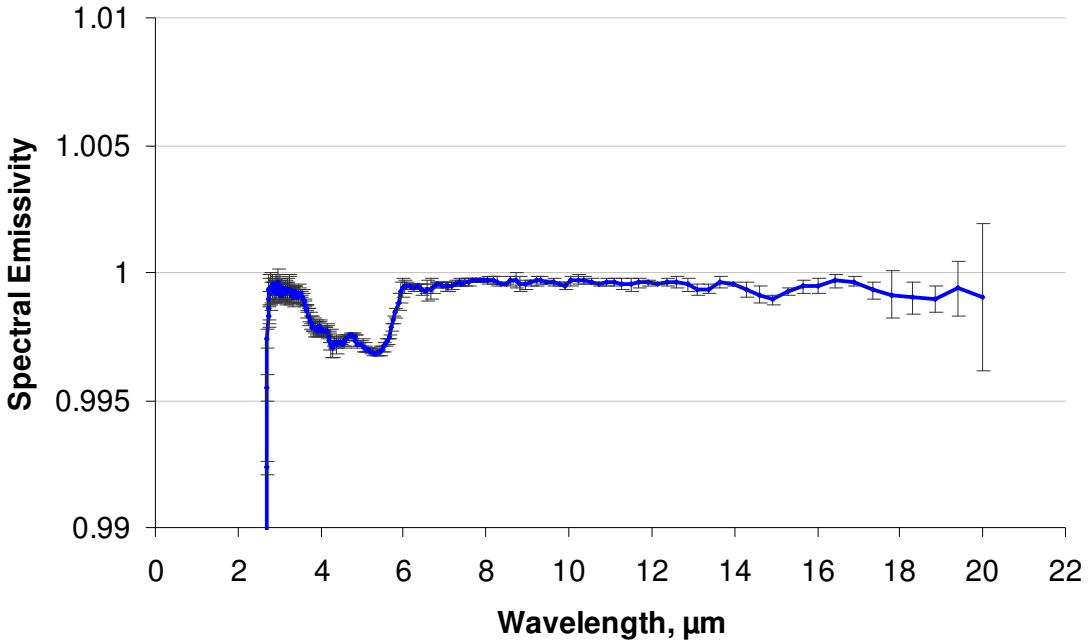


Figure 28. OPMS Type A Uncertainty – Cap Off

The results of the Type B uncertainty analysis will now be discussed. Recall that the OPMS data reduction assumes a spectral emissivity of unity for gold to arrive at the spectral emissivity of the SIRSIII according to

$$\frac{\rho_s(\upsilon)}{\rho_{gold}(\upsilon)}.$$

Since the spectral reflectivity of the SIRSIII is extremely low, a 0.5 to 1.5% bias in the spectral reflectivity of gold has an insignificant effect on the resultant SIRSIII spectral reflectivity and thus, the spectral emissivity. This would not be the case, however, for more highly reflecting samples. The radiation loss due to the mirror hole and the source temperature bias are also negligible since the SIRSIII is very low reflecting. However, when the data taken on the 1614 reference sample was analyzed, a bias in the measured spectral emissivity was present. The spectral scan showed an offset with an absolute

value of 0.01 from the known spectral emissivity distribution. This offset was treated as a bias and was input as Type B uncertainty.

The results of the RSS combination of the uncertainties are shown graphically in Figures 29 and 30 for the measurements with the cap on and off, respectively. It can be seen that in both cases the Type B uncertainty dominates, as was expected. The combined standard uncertainty is nominally 0.01 across the spectrum. Therefore, an expanded uncertainty with k=2 would give a total expanded uncertainty of approximately 0.02 for both data sets. The manufacturer estimates the total uncertainty of the OPMS to be 3% [12]. The details of how that uncertainty value was derived could not be obtained, but this estimate is most likely for higher reflecting samples for which more of the biases that have been presently identified would become significant.

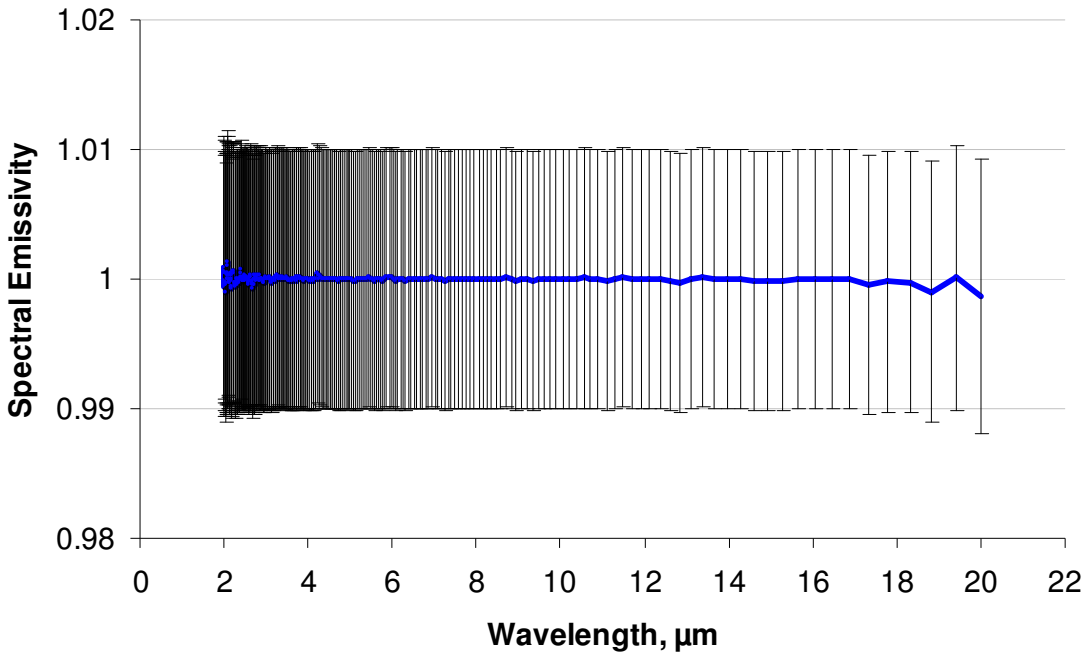


Figure 29. OPMS Combined Standard Uncertainty – Cap On

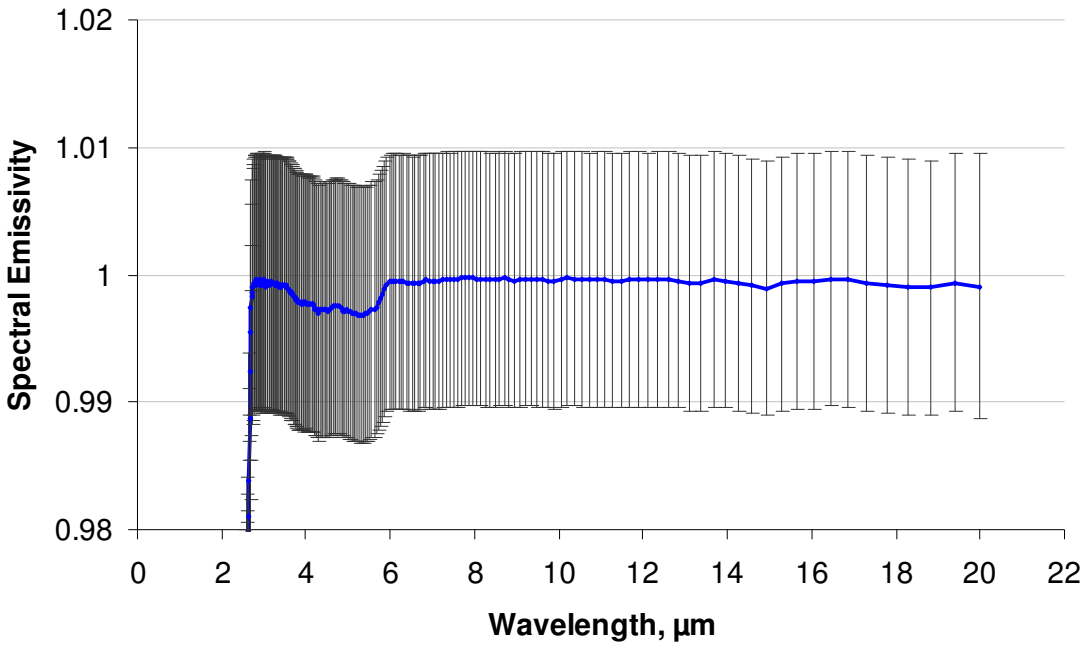


Figure 30. OPMS Combined Standard Uncertainty – Cap Off

4.2.3 Comparison of Measurements and Theories

The results of the theoretical calculations were compared with the OPMS measured spectral emissivities. Figure 31 shows the theoretical calculations compared with the averaged measured spectral emissivities with the reentrant cap on. As discussed earlier, the emissivity of the core is so high that virtually no reflected radiation was detected, resulting in a measured spectral emissivity that hovered around one. The theories also predicted very high emissivities over the 3 to 13 µm wavelength range as being very close to unity and are thus close to the measured values.

Figure 32 shows the comparison for the case with the reentrant cap off and reveals more information regarding the theories and measurements. The data follows the Kelly Method very closely up until 13 µm, after which they diverge and the data follows the

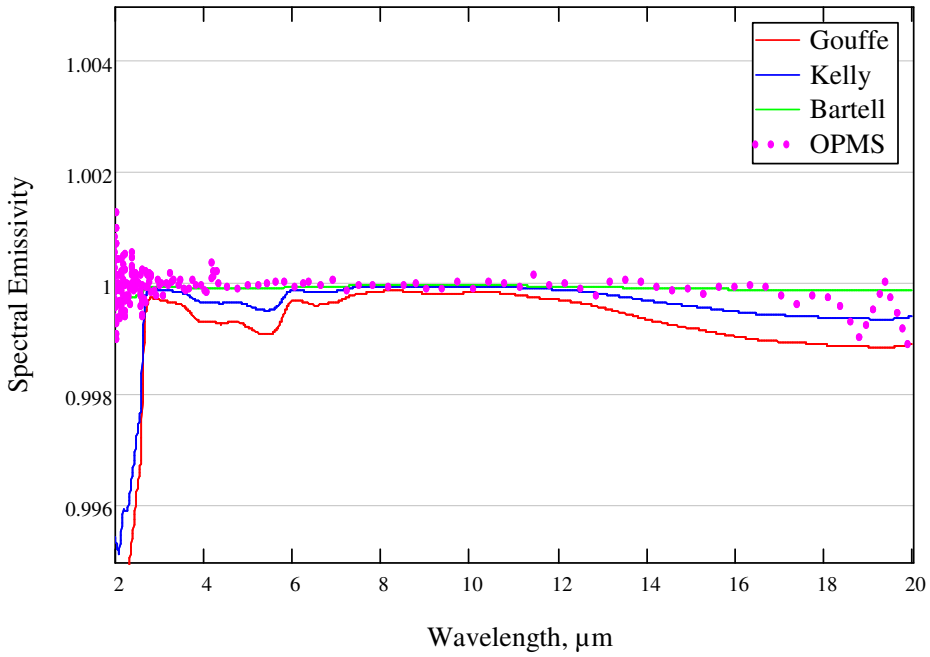


Figure 31. Comparison of OPMS Measurements to Theory – Cap On

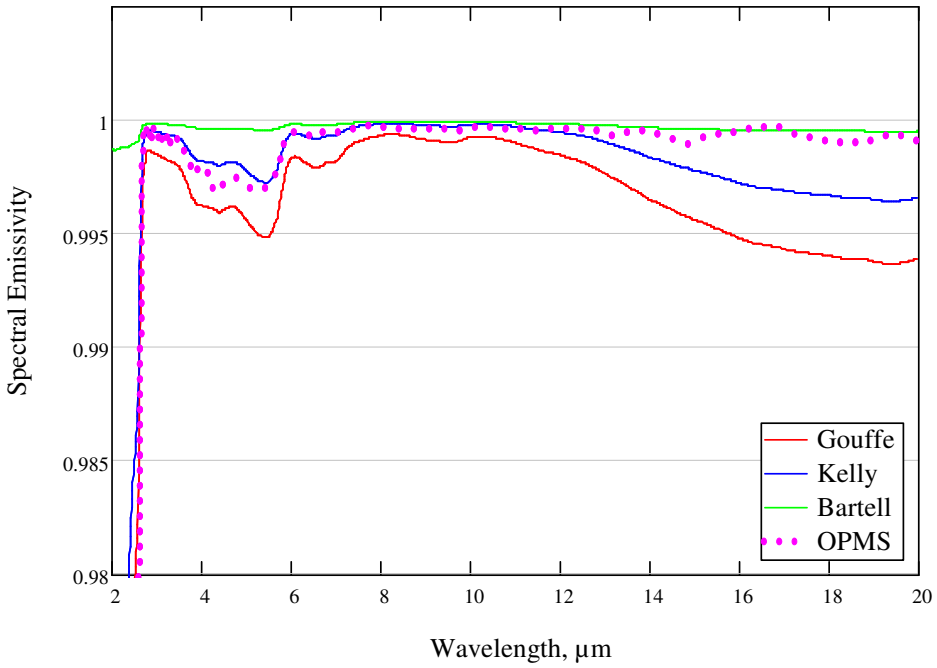


Figure 32. Comparison of OPMS Measurements to Theory – Cap Off

Bartell theoretical calculations. As noted earlier, however, confidence in the measurement data in the longer wavelengths is questionable. The agreement between the measurement data and the theoretical calculations are excellent. Bartell's theory predicted higher values than those measured in the lower wavelength range, but it must be remembered that only a first order approximation of his theory was used in the analysis. As stated earlier, Gouffé's theory predicts the lowest emissivity and does predict lower values than that of the OPMS measurements [1].

4.3 SCAT/R Measurements

4.3.1 Results

The calculated emissivity from the SCAT/R reflectivity data with the reentrant cap on is shown in Figure 33. Figure 34 shows the average of the five runs. Figure 35 shows the cap off data, with the averaged data shown in Figure 36. Both data sets exhibit noisy signal behavior beyond 8μm that would be expected for an extremely low reflecting sample. The data is noisy but averages close to unity.

There is no apparent difference in the data with and without the reentrant cap. The amount of noise present in the instrument masks any differences. As seen with the OPMS data, the differences are small, and cannot be detected with the pyroelectric detector. Pyroelectric detectors output a signal based on the detector material's change in temperature due to incident flux. They operate at room temperature and are known for their low sensitivity.

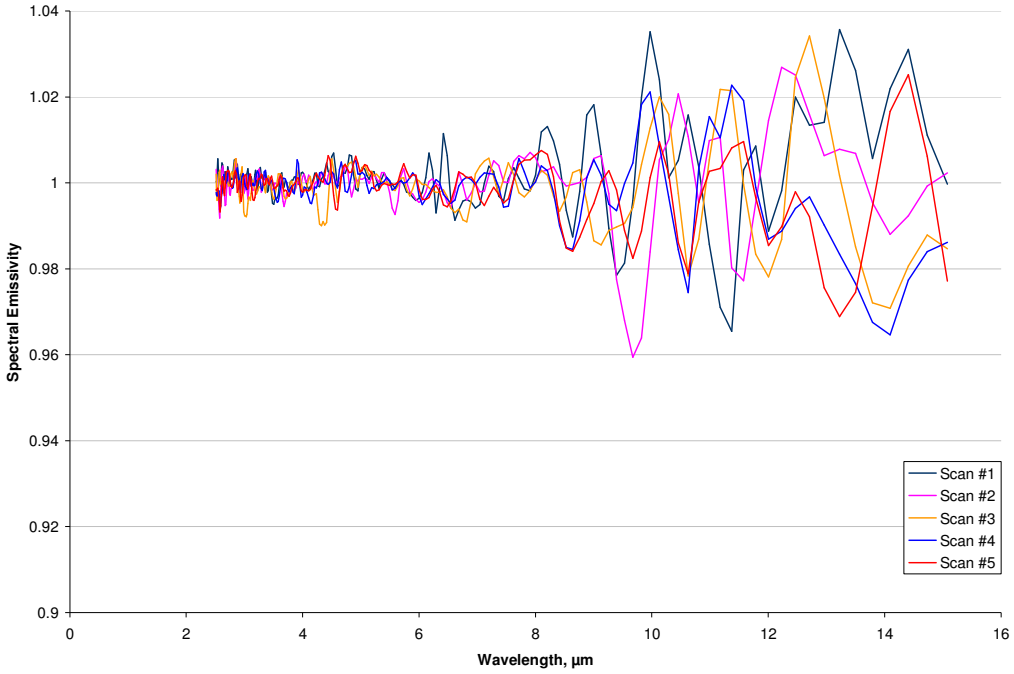


Figure 33. SCAT/R Measured Spectral Emissivity with Reentrant Cap On

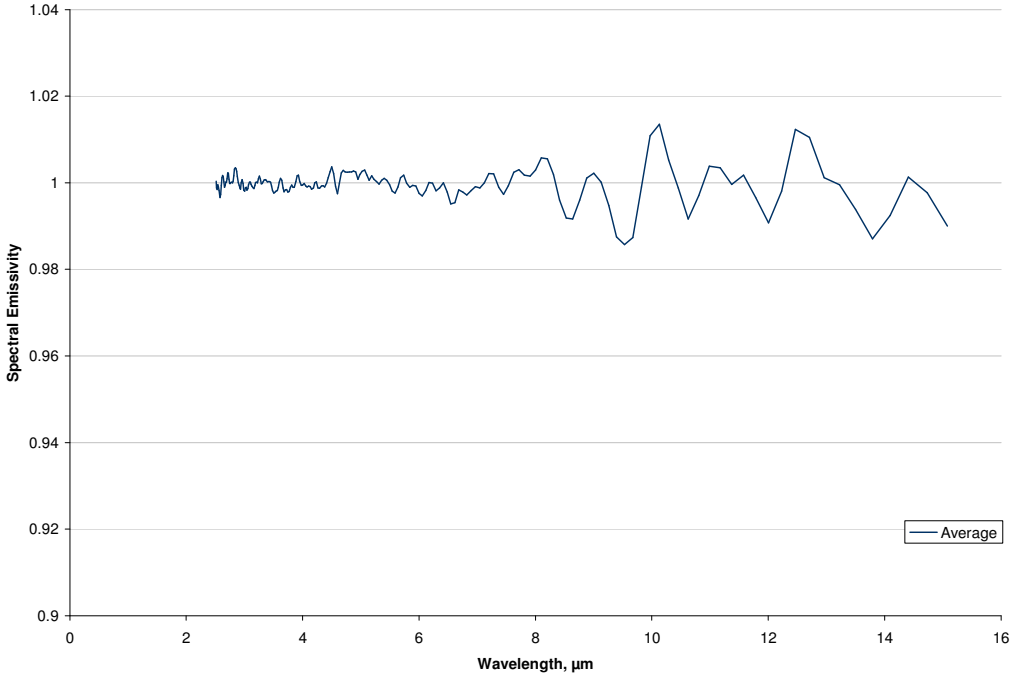


Figure 34. SCAT/R Average Measured Spectral Emissivity with Reentrant Cap On

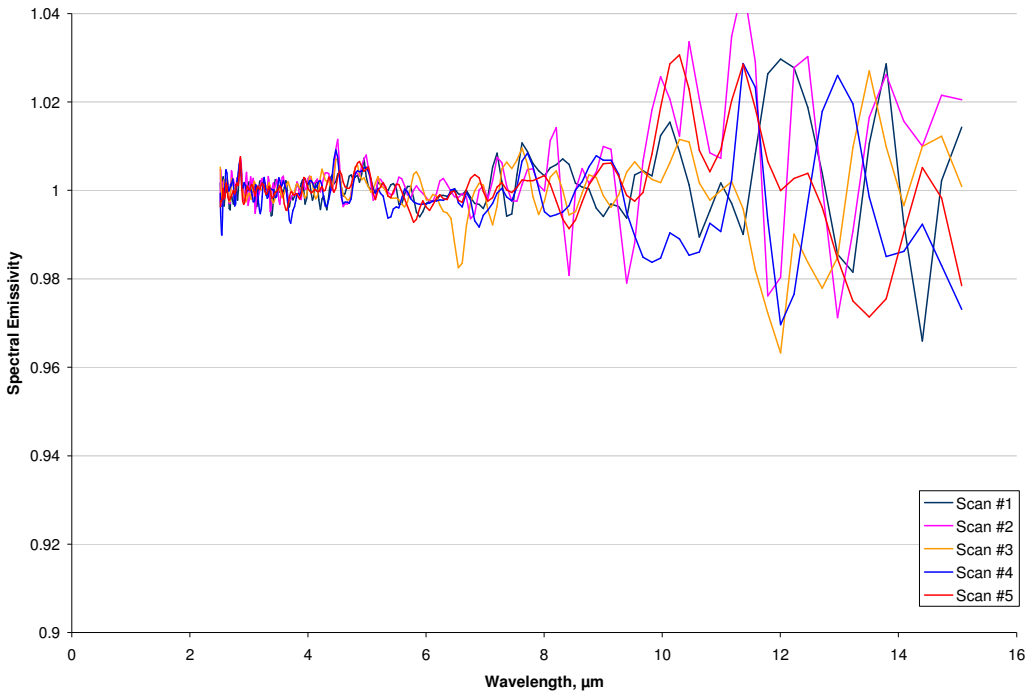


Figure 35. SCAT/R Measured Spectral Emissivity with Reentrant Cap Off

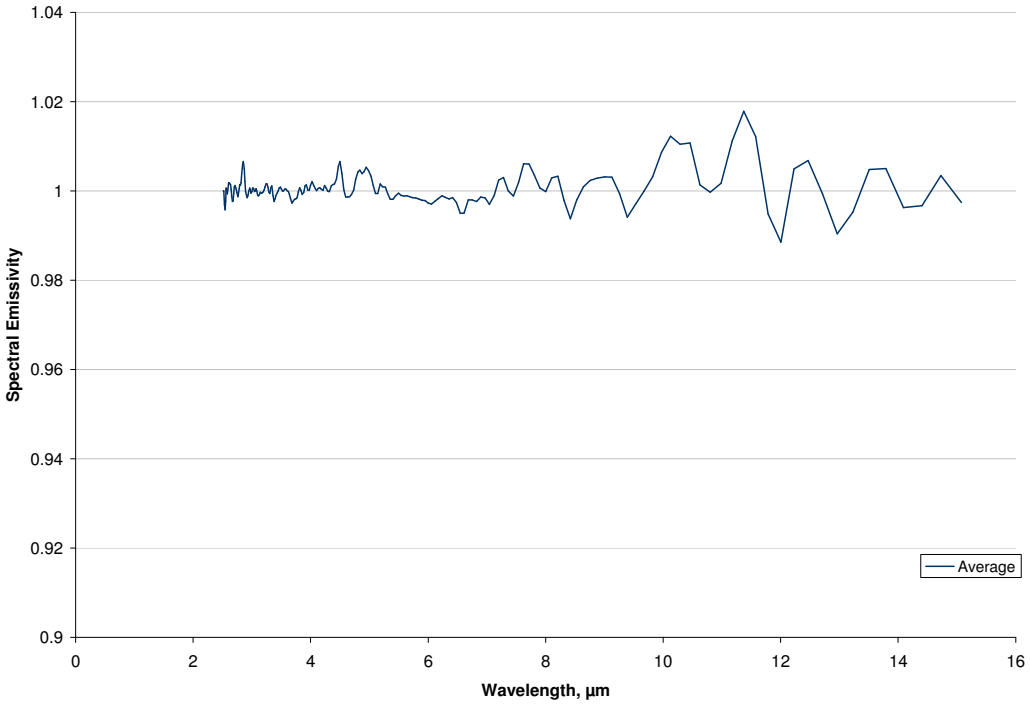


Figure 36. SCAT/R Average Measured Spectral Emissivity with Reentrant Cap Off

It is apparent from the SCAT/R measurements that these types of low signal reflectance measurements need to be performed with a sensitive detector, such as the cryogenic MCT detector in the OPMS. Nevertheless, the SCAT/R measurement data also demonstrates that the cavity is very low reflecting and therefore has a high emissivity.

4.3.2 SCAT/R Data Uncertainty Analysis

The data analysis performed on the data obtained with the SCAT/R instrument will now be discussed. Uncertainties were calculated using the same methodology as the OPMS data. Figures 37 and 38 shows the Type A uncertainty with the reentrant cap on and off respectively.

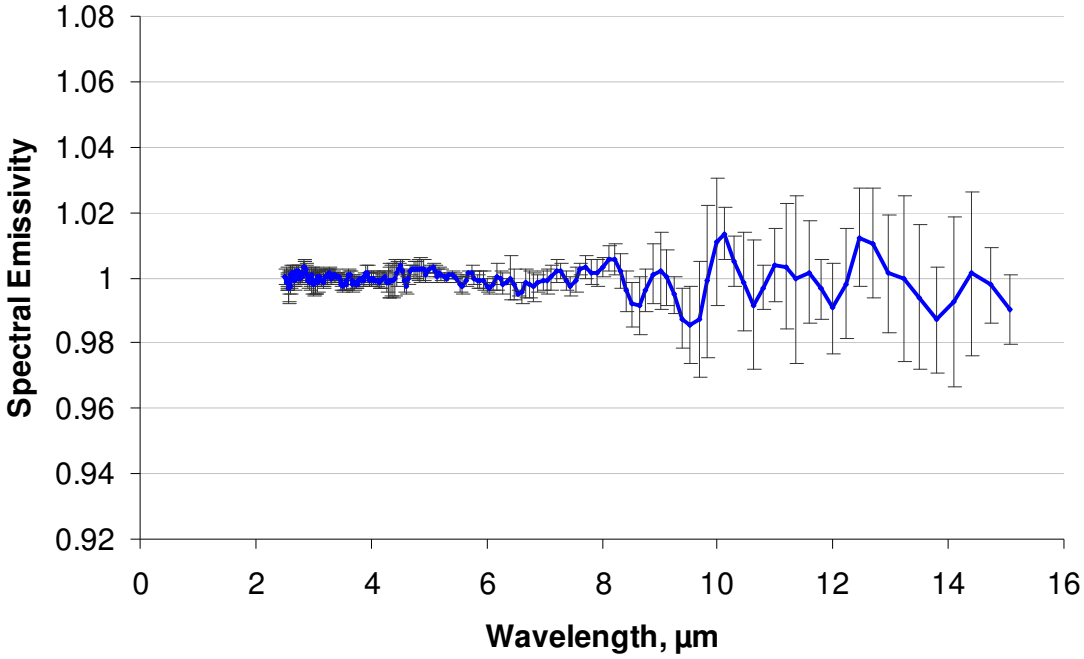


Figure 37. SCAT/R Type A Uncertainty – Cap On

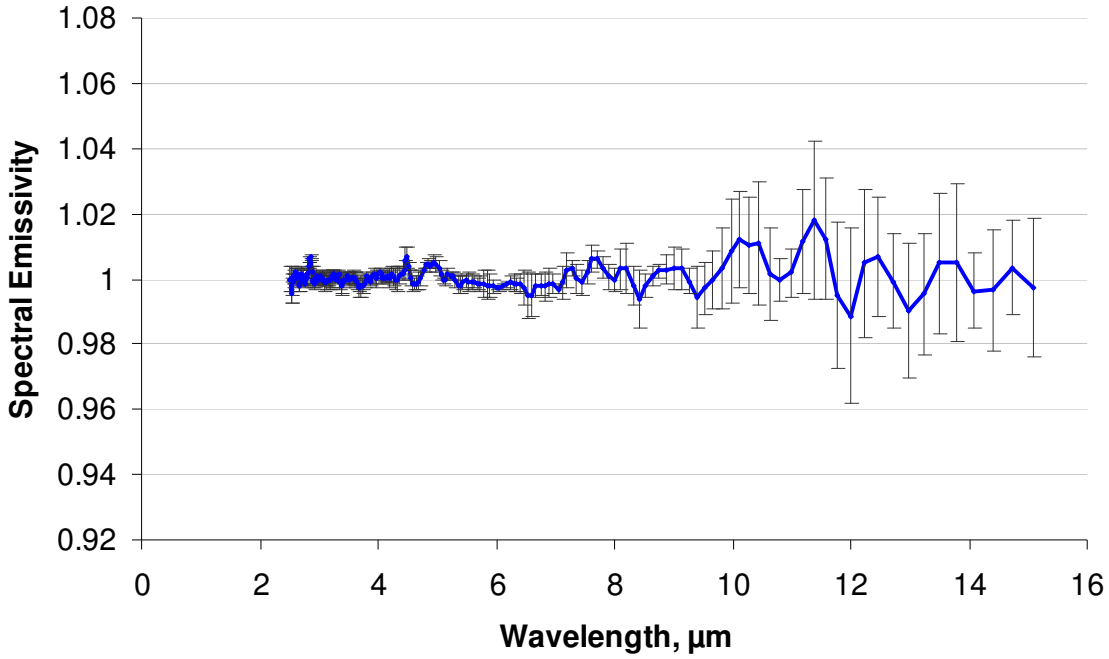


Figure 38. SCAT/R Type A Uncertainty – Cap Off

The results of the Type B uncertainty analysis are as follows. Since the hole loss is 0.0375% of the radiation reflected off the SIRSIII, it is very small since the SIRSIII cavity is very low reflecting and therefore negligible. The calibration uncertainty provided by the manufacturer was an absolute reflectivity of 0.01. This was identified as the only Type B uncertainty and was input into the analysis. The combined standard uncertainty for the data sets is shown graphically for the data with the reentrant cap on and off in Figures 39 and 40, respectively. When a coverage factor of k=2 is applied, the uncertainty grows to approximately 0.02 up to 9 µm and to 0.04 after. This compares well with the manufacturer's expanded uncertainty estimate that resulted in an absolute values of 0.028.

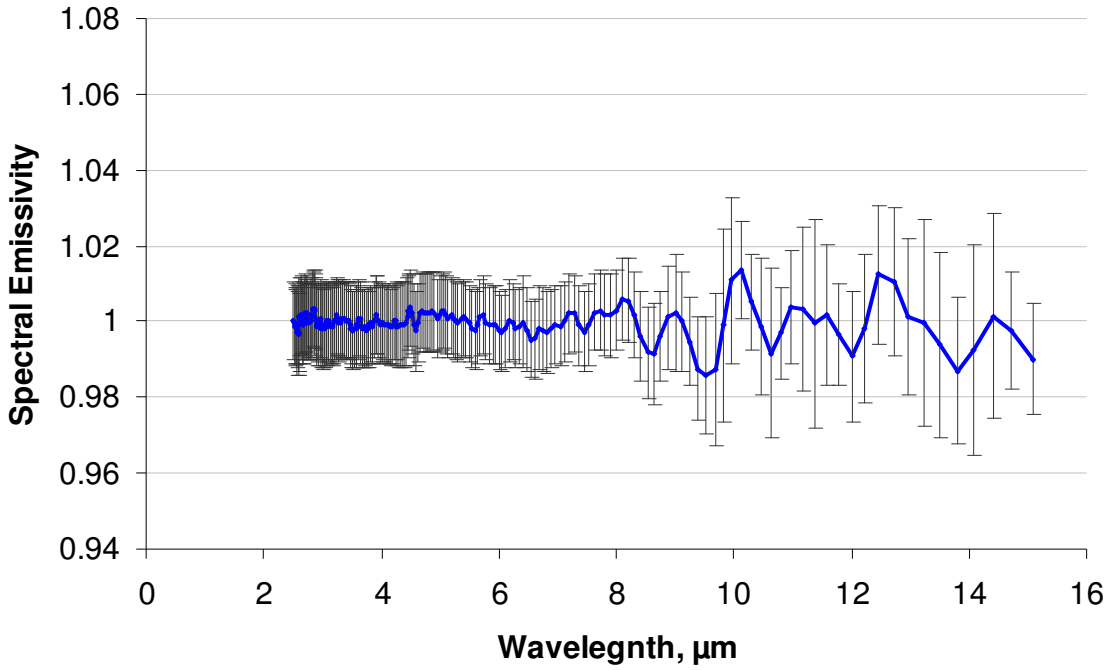


Figure 39. SCAT/R Combined Standard Uncertainty – Cap On

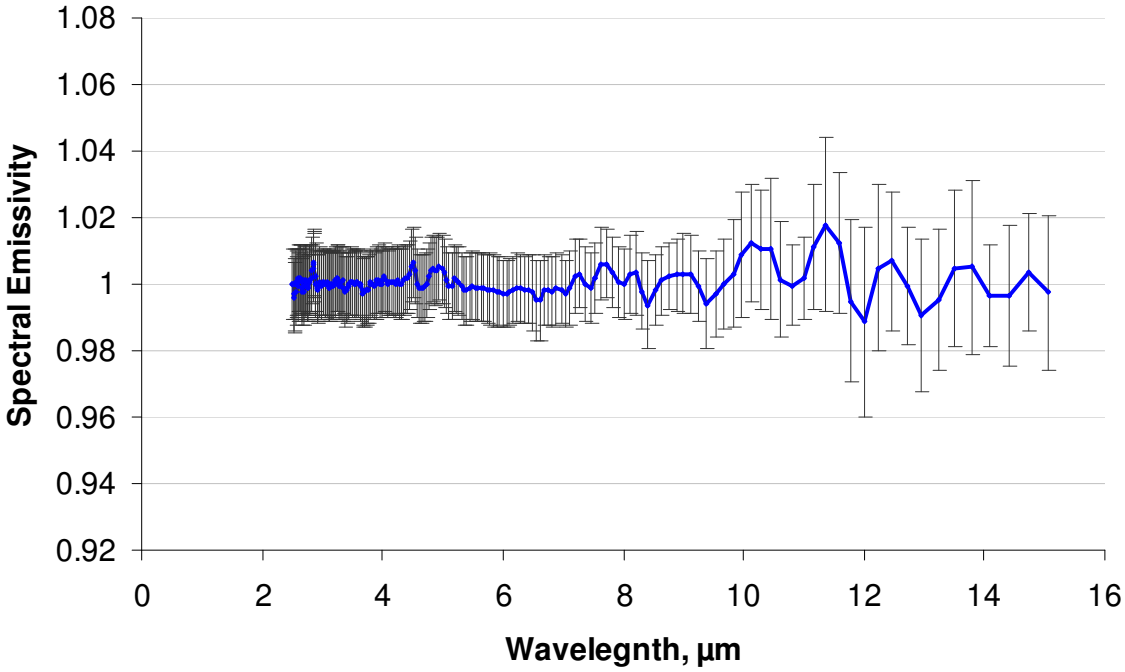


Figure 40. SCAT/R Combined Standard Uncertainty – Cap Off

4.3.3 Comparison of Measurements and Theories

The results of the theoretical calculations previously described in 4.1 were compared with the SCAT/R derived spectral emissivities and will now be presented. The comparisons are not good, as the SCAT/R data has the problems previously discussed. Several data points have noise that is two orders of magnitude greater than the maximum difference in the theories. The comparisons of the theoretical calculations using the Gouffé, Kelly, and Bartell methods and the average measured data are shown in Figures 41 and 42 for the reentrant cap on and off, respectively. Due to the amount of noise present in the measurements, there is little information that can be gained from these comparisons.

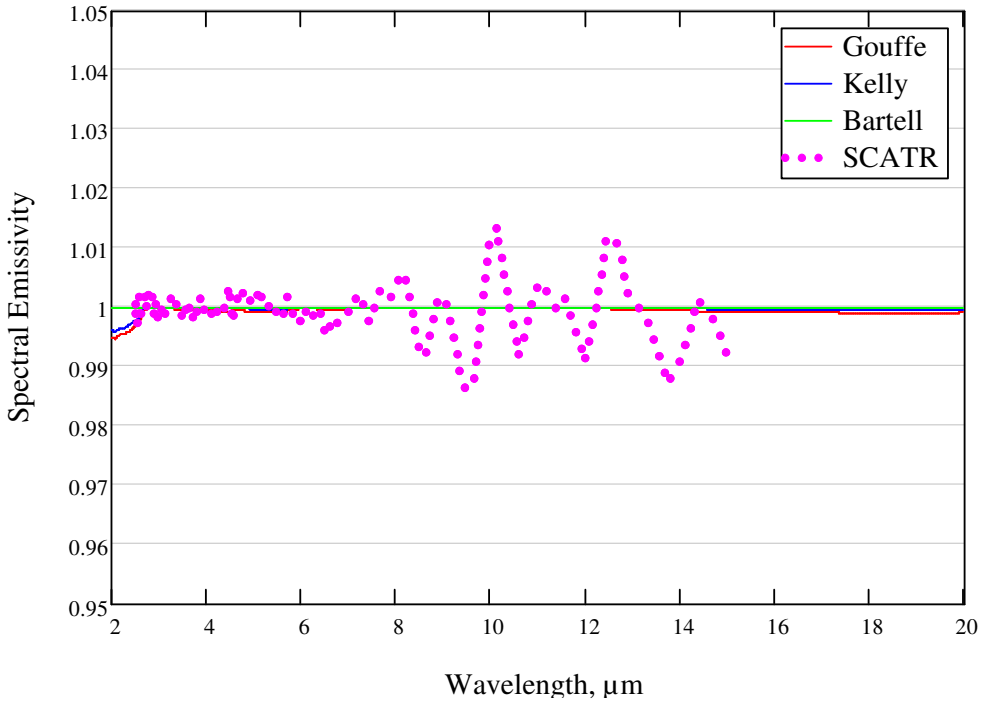


Figure 41. Comparison of SCAT/R Measurements to Theory – Cap On

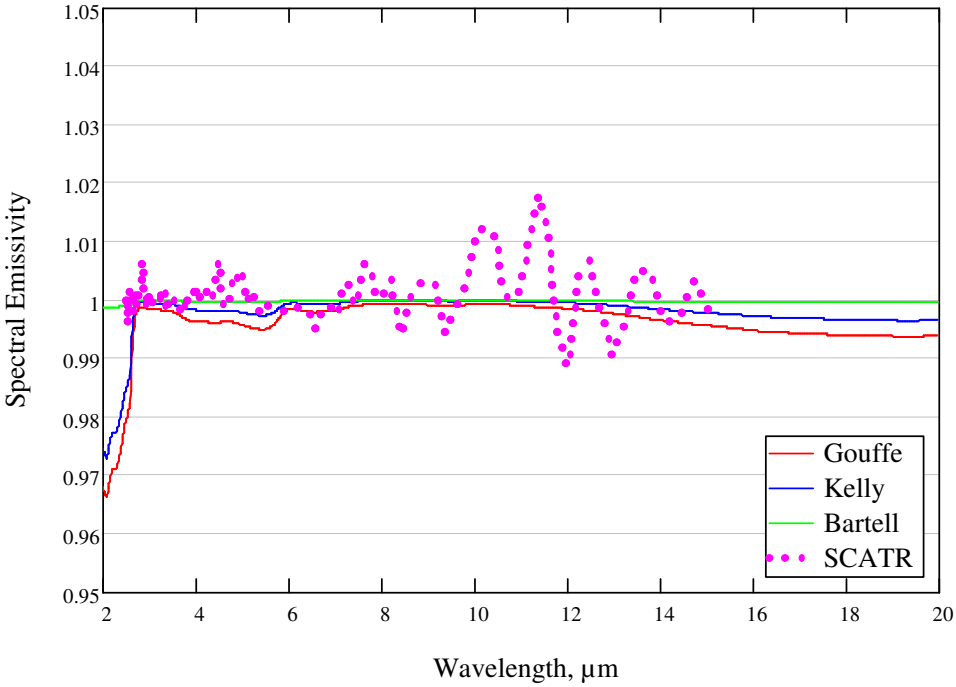


Figure 42. Comparison of SCAT/R Measurements to Theory – Cap Off

4.4 Relation of Measurement Uncertainty to Effective Radiance

The spectral effective radiance of the Standard Source was calculated using the measured spectral emissivity data. The measurement uncertainty was then related to the Standard Source output uncertainty. The results for the OPMS data are shown graphically in Figure 43. When the lower and upper bounds are integrated over the wavelength range to find the effective radiance, both give a 2.002 percent difference in the effective radiance calculated from the mean. The results for the SCAT/R data are shown graphically in Figure 44. When the lower and upper bounds are integrated over the wavelength range, both give a 3.206 percent difference in the effective radiance calculated from the mean. As expected from the uncertainty analysis of the SCAT/R, it gives the highest error in the calculated effective radiance.

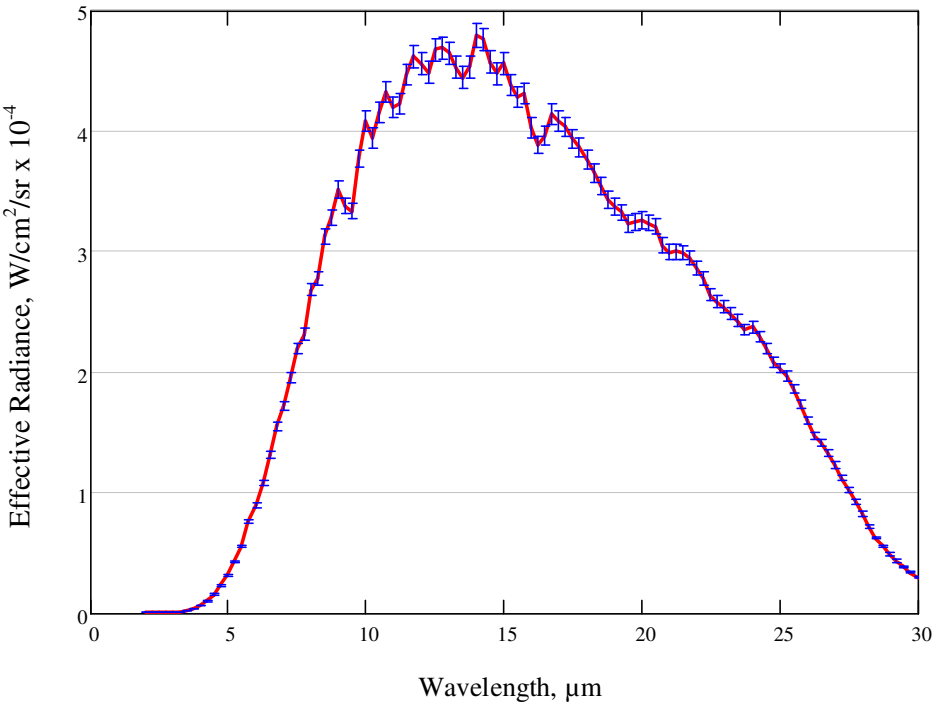


Figure 43. OPMS Data Uncertainty Effect on Effective Radiance

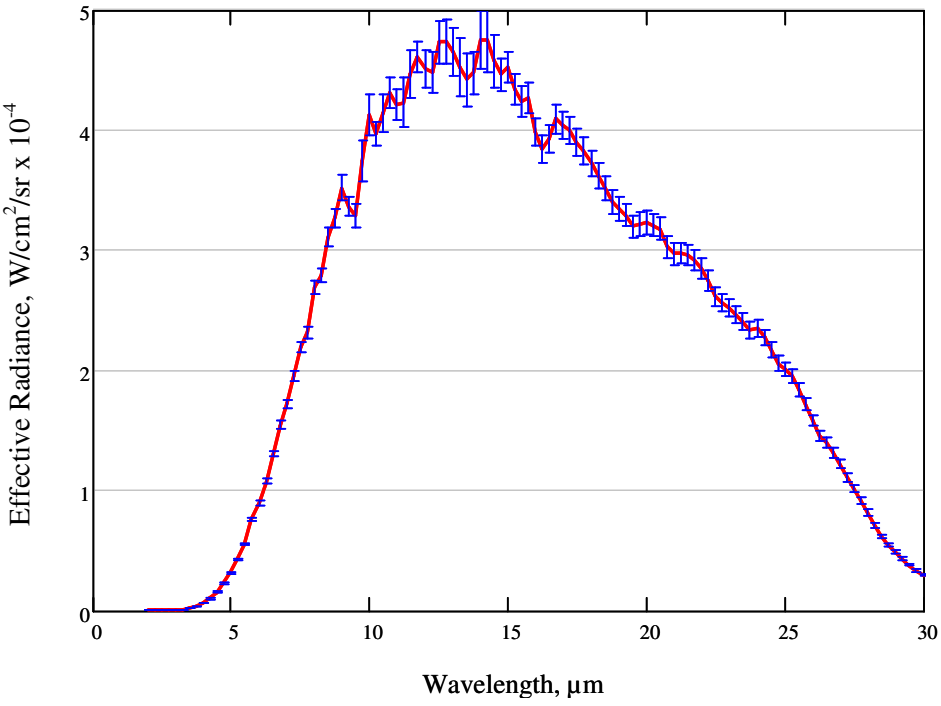


Figure 44. SCAT/R Data Uncertainty Effect on Effective Radiance

Table 4 summarizes the results of the effective radiance calculations for each case. Table 5 shows Standard Source effective radiance data taken in the 7V Chamber [42]. For an ideal blackbody with a total emissivity of unity and at a temperature of 300 K, the effective radiance should be 7.108E-3 W/cm^2/sr and it can be seen that some of the Standard Source data exceeds that value. The effective radiance should be independent of aperture area and less than 7.108E-3 W/cm^2/sr, but errors in the reported aperture sizes, and noise in the detector system between measurements, lead to the variations seen in the data. The average of the data is 7.116E-3 W/cm^2/sr with a standard deviation of 1.568E-05.

Due to the amount of noise and other errors in the 7V Standard Source data, any of the three theories discussed can be used to model the spectral emissivity of the SIRSIII with little difference. The OPMS measurement data can also be used with little error.

Table 4. Summary of Effective Radiances

	Effective Radiance (W/cm^2/sr)		
	Theory	OPMS	SCAT/R
Upper	7.107E-03	7.247E-03	7.281E-03
Mean	7.106E-03	7.105E-03	7.055E-03
Lower	7.104E-03	6.963E-03	6.829E-03

Table 5. Measured Standard Source Effective Radiance Data Taken in 7V Chamber

Aperture Area (cm^2)	Effective Radiance ($W/cm^2/sr$)
0.000250	7.118E-03
0.000503	7.116E-03
0.000984	7.110E-03
0.001470	7.153E-03
0.002010	7.093E-03
0.003310	7.128E-03
0.004530	7.120E-03
0.006370	7.111E-03
0.010100	7.138E-03
0.012600	7.102E-03
0.018800	7.099E-03
0.028600	7.106E-03
0.040500	7.115E-03
0.050600	7.114E-03

CHAPTER V

SUMMARY AND CONCLUSIONS

The research reported in this thesis had two main purposes: model and measure the spectral emissivity of the SIRSIII blackbody simulator cavity design. The results allow a greater understanding of the radiometric properties of this crucial component in the 7V Chamber and are useful for spectro-radiometric modeling.

The cavity emissivity theories of Gouffé, Kelly, and Bartell were extended for spectral use and applied to the SIRSIII cavity. This was done for two cases: 1) with the reentrant cap in place, and 2) with the reentrant cap off. The results of each case were compared. Spectral emissivity measurements using FTIR spectrometry methods were performed using two different instruments at AEDC for both cases. The experimental and theoretical results were compared. An extensive error analysis was performed on the measured emissivity data sets. The uncertainty in the emissivity measurement was then translated into an uncertainty in the output of the Standard Source.

The reentrant cap made measurement of the reflectivity of the cavity very difficult since it caused the SIRSIII to have an extremely low reflectivity. OPMS measurements performed on the SIRSIII with the reentrant cap on were not able to show the structure in the spectral emissivity distribution by the theories but demonstrate the very high emissivity of the cavity. The measurements made with the OPMS for the cap off case produced very good results that compared extremely well with Kelly's theory. The SCAT/R instrument proved to not be well suited for the spectral emissivity measurement.

Of the theories compared, Kelly's resulted in the best model for spectral emissivity over the 2 to 13 μm wavelength range when compared with the OPMS measurements made with the reentrant cap off. Bartell states that Gouffé's errors are serious for conical cavities, but this was not found to be the case in this research. Bartell's calculations were performed for a material with a total emissivity of 0.5. The SIRSIII cavities are constructed of anodized aluminum, a material which has a significantly higher total emissivity than 0.5. While Gouffé's theory did predict low values, they were not significantly lower. It can be concluded that for higher emissivity materials and excellent cavity designs, Gouffé's error becomes less significant. In practice, all three of the theories discussed could be used to model the SIRSIII spectral emissivity with little error, with Kelly's theory having the most accuracy.

Future work should include a more precise spectral emissivity measurement of the SIRSIII cavity using the OPMS by elevating the SIRSIII cavity and instrument source temperatures. This would increase the radiation emitted and reflected from the core and also obtain a higher signal-to-noise ratio. The full form of Bartell's theory should be derived and evaluated for the SIRSIII blackbody simulator, including the weighted configuration factor, and then compared with the theories and measurement data.

REFERENCES

REFERENCES

[1] F. O. Bartell, "Blackbody Simulator Cavity Radiation Theory", Ph. D. Dissertation, University of Arizona, Tucson, Arizona (1978).

[2] H. Lowry, W. Simpson, R. Nicholson, C. Logan, and D. Pruitt, "Using AEDC's Space Chambers for Test and Evaluation of Space Systems," *ITEA Journal*, December 2002/January 2003, pp. 23-29.

[3] H. Lowry, R. Nicholson, R. Simpson, K. Mead, and D. Crider, "Ground Testing of Space-Based Imaging Sensors in AEDC's Space Chambers," AIAA-2004-2194, 24th AIAA Aerodynamic Measurement Technology and Ground Testing Conference, June 28 – July 1, 2004.

[4] H. Lowry, R. Nicholson, R. Simpson, K. Mead, D. Crider, and M. Breeden, "Test and Evaluation of Sensor Platforms in AEDC Space Sensor Test Chambers," AIAA-2005-7634, U.S. Air Force T and E Days, Nashville, Tennessee, Dec. 6-8, 2005.

[5] H. Lowry, W. Goethert, W. Bertrand, and D. Crider, "Continued Development and Integration of Scene Projection Technologies in the AEDC Space Simulation Chambers," in Proceedings of SPIE Vol. 5075 *Targets and Backgrounds IX: Characterization and Representation*, edited by Wendell R. Watkins, Dieter Clement, William R. Reynolds, (SPIE, Bellingham, WA, 2003) pp. 300-311.

[6] H. Lowry, D. Crider, W. Goethert, and W. Bertrand, "Implementation of Scene Simulation Technologies in the AEDC Space Chambers," in Proceedings of SPIE Vol. 5408 *Technologies for Synthetic Environments: Hardware-in-the-Loop Testing IX*, edited by Robert Lee Murrer, (SPIE, Bellingham, WA, 2004) pp. 84-95.

[7] D. Crider, H. Lowry, R. Nicholson, and K. Mead, "Uncertainty Analysis of the 7V Chamber," in *Infrared Imaging Systems: Design, Analysis Modeling, and Testing XVI*, edited by Gerald C. Holst, Proceedings of SPIE, Vol. 5874 (SPIE, Bellingham, WA, 2005), pp. 289-300.

[8] D. Crider, H. Lowry, and R. Young, "Blackbody Characterization and Analysis for Infrared Scene Projection," in *Technologies for Synthetic Environments: Hardware-in-the-Loop Testing XI*, edited by Robert Lee Murrer, Proceedings of SPIE Vol. 6208 (SPIE, Bellingham, WA, 2006), 620819.

[9] C. Herron, S. Steely, and R. Young, "Arnold Engineering Development Center Low-Background Blackbody Calibration," AEDC-TR-93-17, November 1993.

[10] R. J. Chandos, and R. E. Chandos, “Radiometric properties of isothermal, diffuse wall cavity sources,” *Appl. Opt.* 13, 2142- (1974).

[11] R. Bedford, and C. Ma, “Emissivities of diffuse cavities. III. Isothermal and nonisothermal double cones,” *J. Opt. Soc. Am*. 66, 724- (1976).

[12] J. R. Markham, K. Kinsella, R. M. Carangelo, C. R. Brouillette, M. D. Carangelo, P. E. Best, and P. R. Solomon “Bench top Fourier transform infrared based instrument for simultaneously measuring surface spectral emittance and temperature,” *Rev. Sci. Instrum.* 64, 2515– (1993).

[13] E. Lindermeir and V Tank, “The spectral emissivity of natural surfaces measured with a Fourier transform infrared spectrometer,” *Measurement* 14, 177– (1994).

[14] M. J. Ballico and T. P. Jones, “Novel experimental technique for measuring high-temperature spectral emissivities,” *Appl. Spectrosc*. 49 335– (1995).

[15] L. Hanssen, S. Mekhontsev, and V. Khromchenko, “Infrared Spectral Emissivity Characterization Facility at NIST,” in Proceedings of SPIE Vol. 5405 *Thermosense XXVI*, edited by Douglas D. Burleigh, K. Elliott Cramer, G. Raymond Peacock, (SPIE, Bellingham, WA, 2004), pp. 1-12.

[16] V. I. Sapritsky and A. V. Prokhorov, "Spectral effective emissivities of nonisothermal cavities calculated by the Monte Carlo method," *Appl. Opt.* 34, 5645- (1995).

[17] L. D. Kirkpatrick and G. F. Wheeler, *Physics: A World View*, 2nd ed., Saunders College Publishing, 1995.

[18] L. M. Smith, *Fundamental Principles of Optical Engineering*, University of Tennessee Space Institute, Tullahoma, TN, 1993 (unpublished).

[19] P. J. Nolan, *Fundamentals of College Physics*, Wm. C. Brown, Dubuque, Iowa, 1993.

[20] J. D. Vincent, *Fundamentals of Infrared Detector Operation and Testing,* Wiley, New York, NY, 1990.

[21] F. O. Bartell, “A blackbody, a blackbody simulator, a blackbody simulator cavity, a blackbody simulator cavity aperture, and a blackbody simulator aperture are each different from one another,” in *Imaging Infrared: Scene Simulation, Modeling, and Real Image Tracking*, edited by August J. Huber, Milton J. Triplett, James R. Wolverton, Proceedings of SPIE, Vol. 1110 (SPIE, Bellingham, WA, 1989) 183- (1989).

[22] A. J. LaRocca, “Artificial Sources,” The *Infrared and Electro-Optical Systems Handbook-Volume 1: Source of Radiation*, edited by G. J. Zissis, SPIE and ERIM (1993).

[23] R. J. Chandos and R. E. Chandos, “Radiometric properties of isothermal, diffuse wall cavity sources,” *Appl. Opt*. 13, 2142- (1974).

[24] F. O. Bartell and W. L. Wolfe, “A comparison of the performance of blackbody simulators of different shapes,” Proceedings of the Technical Program, Electro-Optical Systems Design Conference, San Francisco, CA, November 5-7, 103- (1974).

[25] D. Moore, “Investigation of Shallow Reference Cavities for High-Temperature Emittance Measurements” in *Measurement of Thermal Radiation Properties of Solids*, NASA SP-31, edited by J. C. Richmond, NASA, Washington, D. C. (1963).

[26] F. J. Kelly, "An equation for the local thermal emissivity at the vertex of a diffuse conical or V-groove cavity," *Appl. Opt.* 5, 925- (1966).

[27] F. O. Bartell and W. L. Wolfe, “Cavity radiators: an ecumenical theory,” *Appl. Opt.* 15, 84- (1976).

[28] F. J. Kelly and D. G. Moore, "A test of analytical expressions for the thermal emissivity of shallow cylindrical cavities," *Appl. Opt*. 4, 31- (1965).

[29] B.C. Smith, *Fourier Transform Infrared Spectroscopy*, CRC Press, Boca Raton, FL, 1996.

[30] J. W. Goodman, *Statistical Optics*, John Wiley and Sons, New York, 1985.

[31] S. A. Stepanek, “Measuring wavelength and temperature dependencies of material optical properties,” AIAA-95-2035, 30th AIAA Thermophysics Conference, San Diego, CA, June 19-22, 1995.

[32] D. Crandall, “SCAT/R Operation Manual,” AZ Technology (2001).

[33] Stuart Coulter, Aerospace Testing Alliance, Arnold Engineering Development Center, personal communication.

[34] Mathsoft Engineering and Education, Inc., *Mathcad 13 User’s Guide* (“Mathcad” is a registered trademark of Mathsoft), Mathsoft Engineering and Education, Inc., Cambridge, Massachusetts.

[35] Galactic Industries Corporation, *Spectra Calc User's Guide* ("Spectra Calc" is a registered trademark of Galactic Industries), Galactic Industries Corporation, Salem, New Hampshire.

[36] Galactic Industries Corporation, *GRAMS/32 User's Guide* ("GRAMS/32" is a registered trademark of Galactic Industries), Galactic Industries Corporation, Salem, New Hampshire.

[37] B. N. Taylor and C. E. Kuyatt, "Guidelines for evaluating and expressing the uncertainty of NIST measurement results," National Institute of Standards and Technology Technical Note 1297, Gaithersburg, MD, September 1994.

[38] ISO, *Guide to the Expression of Uncertainty in Measurement*, International Organization for Standardization, Geneva, Switzerland, 1993.

[39] S. A. Stepanek, "Measuring wavelength and temperature dependencies of material optical properties," AIAA-95-2035, 30th AIAA Thermophysics Conference, San Diego, CA, June 19-22, 1995.

[40] H. S. Lowry, W. H. Goethert, S. L. Steely, W. R. Simpson, D. H. Crider, and M. F. Breeden, "Optical coating considerations for cryogenic mirrors used in AEDC's 7V and 10V space sensor test chambers," in *Cryogenic Optical Systems and Instruments XI* edited by James B. Heaney and Lawrence G. Burriesci, Proceedings of SPIE Vol. 5904 (SPIE, Bellingham, WA, 2005), 59040R.

[41] B. E. Wood, J. G. Pipes, A. M. Smith, and J. A. Roux, "Hemi-ellipsoidal mirror infrared reflectometer: development and operation," *Appl. Opt*. 15, 940- (1976).

[42] Kimberly Mead, Aerospace Testing Alliance, Arnold Engineering Development Center, personal communication.

VITA

Dustin Crider was born in Paducah, KY in 1980 and raised in the small town of Milburn, KY. He received the Bachelor of Science Degree in Physics from Murray State University in 2002. There he received the Outstanding Physics Senior Award and graduated Summa Cum Laude. He has been employed as a contractor at the Arnold Engineering Development Center since May 2002. He enrolled at UTSI that fall. His professional experience includes radiometric system analysis, optical component measurement and analysis, infrared scene projection, optical systems alignment, space environment simulation, charged particle beams and diagnostics, electro-optic systems, and data analysis. He received the Master of Science degree in August 2006.